THE UNIVERSITY
of EDINBURGH

THE UNIVERSITY *of* EDINBURGH
School of Biomedical Sciences

Investigating the Molecular Basis of Motor Neuron Vulnerability in Mouse Models of Spinal Muscular Atrophy

Natalie Louise Courtney

s1476172

Primary Supervisor: Dr Lyndsay Murray
Secondary Supervisor: Dr Paul Skehel

Master of Science by Research

September 2014 - August 2015

Abstract

Spinal Muscular Atrophy (SMA) is a motor neuron disease that predominantly affects children, with the most severe form of SMA resulting in death before the age of 2 years. It is an autosomal recessive disorder that leads to progressive paralysis and muscle atrophy due to the degeneration of lower motor neurons. Furthermore, a loss of the connections between motor neurons and muscle (neuromuscular junctions; NMJs) occurs early in the disease. Importantly, not all motor neurons are equally affected. For example, in specific mouse models of SMA, there is a high level of NMJ loss in the abdominal muscles while NMJs within cranial muscles remain intact, even at late stages of disease. Prior to this study, RNAseq analysis of differentially vulnerable motor neurons in the *Smn*$^{2B/-}$ mouse model of SMA, and in wild-type mice, was carried out at a pre-symptomatic stage. In this project, there are two main aims. Firstly, transcriptional changes that occur between differentially vulnerable motor neurons were further investigated. qRT-PCR was used to detect transcriptional changes that occur between *Smn*$^{2B/-}$ and wild type mice and immunofluorescence was used to detect protein markers of transcripts that were altered in vulnerable motor neurons. qRT-PCR confirmed changes in Ubiquitin as well as transcripts associated with cell death. Immunofluorescence analysis showed no significant change in protein markers of DNA repair between differentially vulnerable motor neuron populations. Secondly, the activation of a cell death pathway in a mouse model of SMA was investigated. For this aim, the *Smn*$^{2B/-}$ mouse line was re-derived and preliminary phenotypic assessment was preformed. The re-derived model displays similar features to the original *Smn*$^{2B/-}$ mouse model of SMA. In addition, the incidence and timing of cell death pathway activation was investigated by qRT-PCR. This showed an up-regulation of transcripts involved in cell death pre-symptomatically. Up-regulation of these transcripts at this time point suggests that the activation of cell death pathways may contribute to motor neuron degeneration and therefore warrants further investigation.

Lay Summary

Motor neurons are long cells that connect the spinal cord to muscles, instructing the muscles to contract. In motor neuron diseases, like Spinal Muscular Atrophy (SMA), these cells breakdown and the connection to the muscle (neuromuscular junction) is destroyed. In SMA, some motor neurons in the body are resistant, and even at a late stage in the disease the neuromuscular junction does not breakdown. To date, it is not known why some motor neurons are resistant. Prior to this project, work found differences between motor neurons of healthy mice and SMA-like mice. It also, found differences between the motor neurons that breakdown and the motor neurons that don't. In this project, we wanted to confirm these differences. In addition, we found that in the motor neurons that breakdown, the switch that tells them to die has been turned on early, before there appears to be anything physically wrong with the cell. Perhaps, if the turning on of this switch is delayed, the breakdown of the motor neuron will be postponed. We suggest this idea should be investigated further.

Acknowledgements

I would like to thank Dr Lyndsay Murray for giving me the opportunity to carry out this work within her laboratory. Her help, support and inspiration throughout has been invaluable.

Thank you to all of the short-term members of the Murray Laboratory, all members of the Gillingwater Laboratory and to Dr Paul Skehel for their help and advice.

Many thanks must also go to the University of Edinburgh Anatomy Department and the Gwendolyn Strong Foundation for allowing me to study for an MSc by Research.

In loving memory of Nancy Mackie
(1941 - 2015)

Declaration

Unless otherwise acknowledged, the work presented here is entirely my own and has not been submitted for any other qualification.

Natalie Courtney
August 2015

Table of Contents

Chapter 1: Introduction

Spinal Muscular Atrophy (SMA) is a devastating motor neuron disease that affects primarily children. It is an autosomal recessive disorder that leads to progressive paralysis and muscle atrophy due to the degeneration of lower motor neurons. With a carrier frequency of 1 in 35 and an incidence of 1:6000, it is the most common genetic cause of infant mortality.[1] The most severe form of SMA results in death before the age of 2 years however the levels of severity that manifest can vary substantially.[2] Despite this debilitating and distressing disorder affecting a relatively high population there is, to date, no known treatment or cure for SMA.

SMA is caused by a mutation or deletion of the Survival Motor Neuron 1 (*SMN1*) gene resulting in a decrease in Survival Motor Neuron (SMN) protein.[3,4] As well as *SMN1*, humans possess another *SMN* gene, *SMN2*, which has an alternative pre-mRNA splicing pattern due to a C-T transition in exon 7.[5] Therefore, the majority of *SMN2* product is a reduced length, short lived and non-functional SmnΔ7 protein, with only 10-15% of *SMN2* product being full length SMN.[6,7] There is variation in the number of copies of *SMN2* within the human genome and since *SMN2* copy number is proportional to the level of full length SMN produced, the copy number is a determinant of disease severity.[8]

Although SMN is a ubiquitous protein, motor neurons are selectively vulnerable when SMN is reduced and they degenerate as a result.[9] The reasons for this selective vulnerability of motor neurons are still unclear but perhaps a cellular threshold exists and SMN levels in SMA are lower than that required by motor neurons.[4,10] This theory is supported by reports that severe SMA patients, who will have the lowest levels of SMN protein, can present with heart defects that are not observed in patients with less severe forms of SMA, who will have increased levels of SMN protein.[11] This suggests that the heart can also be susceptible to low SMN but its threshold is greater than the threshold of motor neurons.[4] The degeneration of motor neurons is initially apparent at the neuromuscular junctions (NMJs), the connection between the axon of a lower motor neuron (pre-synaptic terminal) and the endplate of a muscle fiber (post-synaptic terminal).[9] There have been reports of various

abnormalities at these junctions in SMA; they fail to mature and as the disease progresses there is an accumulation of neurofilaments (NFs) at the pre-synaptic terminal as well as denervation of endplates and pre-synaptic terminal sprouting.[9,12]

Further to this selective vulnerability, specific subsets of motor neurons are more vulnerable to low SMN than others and while some degenerate others are resistant and remain in tact, even at the end stage of the disease.[9,13,14] For example, motor neurons that supply muscles of the abdomen degenerate while motor neurons supplying cranial muscles do not.[15,16] Again, the reasons for this are still unclear. Murray *et. al.* (Acta Neuropathol. Commun., *In Press*) performed transcriptional analysis of these differentially vulnerable motor neurons to address why some are more susceptible to degeneration.[15] They asked two main questions (Figure 1). Firstly, what transcriptional changes occur when SMN is reduced? For this they compared SMA mouse model motor neurons to wild type mice motor neurons. In their comparison they used two distinct motor neuron populations, the thoracic spinal cord motor neurons, that supply abdominal muscles and are vulnerable in SMA, and brainstem motor neurons, that supply cranial muscle and are resistant in SMA (Figure 1: blue arrows). By having two comparisons, they were able to filter the transcriptional changes that occurred in both, lowering the number of transcriptional changes that were most likely caused by reduced SMN and were therefore of interest. Secondly, they asked what transcriptional changes occur in vulnerable motor neurons that may make them degenerate? To answer the second question they compared the vulnerable SMA motor neurons that degenerate to motor neurons that don't degenerate. Those that don't degenerate and were used as comparisons were resistant SMA motor neurons and wild type vulnerable motor neurons (Figure 1: red arrows). Again, they filtered for transcriptional changes that were common in the two comparisons.

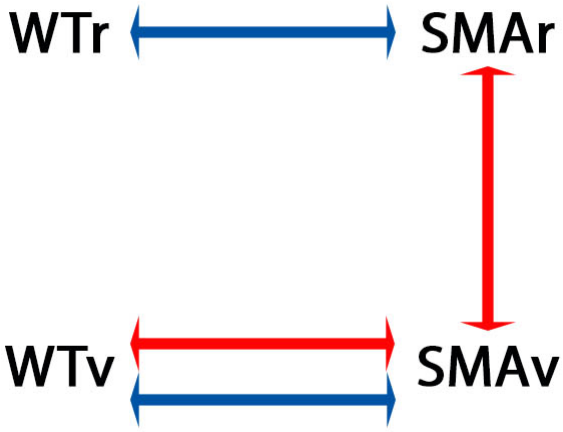

Figure 1: A comparison of differentially vulnerable motor neurons carried out by Murray et. al. *Blue arrows*: WTr and SMAr motor neurons and WTv and SMAv motor neurons were compared to discover transcripts that are altered by a reduction in Smn. *Red arrows*: SMAv and Wtv motor neurons and SMAv and SMAr motor neurons were compared to discover alterations in transcripts that may provide resistance to degeneration. (Diagram adapted from Murray et. al.; WTr – Wild type resistant, WTv – Wild type vulnerable, SMAr – SMA model resistant, SMAv – SMA model vulnerable)

Prior to the work by Murray *et. al.* (Acta Neuropathol. Commun., *In Press*), other studies had carried out transcriptional analysis on SMA mouse models. Zhang *et. al.* (2008) compared the transcriptional profiles of the spinal cords, as well as the brain and kidneys, of severe SMA mouse models to control mice, by microarray.[17] This may provide information of transcripts altered by a reduction in SMN however, it does not shed light on why motor neurons in SMA are differentially vulnerable. Furthermore, microarray analysis is less accurate and sensitive to transcriptional changes than RNAseq.[18] In comparison, Staroploi *et. al*. (2015) used RNAseq analysis rather than microarray but still only compared the profiles of SMA mouse model and control tissue.[19] However, they did analyse the transcriptional profiles at various time points, which spanned pre-symptomatic and symptomatic stages. This aimed to account for transcriptional changes that occur due to developmental progression. Nevertheless, the work by Murray *et. al.* is unique. They compare very different and distinct motor neuron populations in an SMA mouse model and wild type mice and by screening for common transcriptional changes that occurred in two screens, both of which could answer the same question, they dramatically reduced the number of transcripts that could be important in causing the disease pathology. In addition, they look at the transcriptional profiles of these motor neuron populations

at a pre-symptomatic time point, before the SMA mouse model is displaying any pathological markers of SMA. In the *Smn*$^{2B/-}$ mouse model of SMA, which was used in their work, this time point was P10.[20] Therefore, the work by Murray *et. al.* gives an insight into possible genetic changes that occur in mouse models of SMA that could influence the onset of pathology.

There are a number of mouse models of SMA that vary in their severity. The *Smn*$^{2B/-}$ mouse model of SMA is an intermediate mouse model of SMA that traditionally has a lifespan of approximately 28 days.[20] Mice lack the *SMN2* gene, which is found only in humans and therefore the SMA phenotype of this model is established through the genetic modification of the murine *Smn* gene. The *Smn2B* allele of the gene acts like *SMN2*, due to a mutation within exon 7, and when expressed on a null background creates a mouse with a phenotype representative of SMA.[21] The null background is created by inserting a neomycin cassette within exon 2 and is embryonic lethal without the addition of genetic substitutions that can produce at least a little SMN protein.[22] Another, more severe mouse model of SMA is the *Smn*$^{-/-}$;*SMN2*$^{(tg/0)}$ model, which has a lifespan of 10 days.[23] This mouse model of SMA is created through the addition of *SMN2* onto a null background however, this null background is created by inserting a cassette into exon 7 rather than exon 2.[23]

Aims

In this project, I had the following aims:

Aim 1: ***Investigating transcriptional differences between differentially vulnerable motor neurons***

Firstly, I aimed to detect transcriptional changes that were identified by RNAseq by either qRT-PCR or immunofluorescence. qRT-PCR was used to detect transcriptional changes that occur in the $Smn^{2B/-}$ mouse model of SMA compared to wild type motor neurons. Immunofluorescence was used to detect protein markers of transcripts that were altered in vulnerable motor neurons compared with resistant motor neurons.

Aim 2: ***Re-deriving the $Smn^{2B/-}$ mouse model for investigation into cell death pathway activation***

Secondly, I aimed to re-derive the $Smn^{2B/-}$ mouse model of SMA in order to investigate cell death pathway activation. This SMA mouse model was created by crossing $Smn^{2B/+}$ mice, on a C57BL6J background, with $Smn^{+/-}$ mice, on a FVB background. This $Smn^{2B/-}$ mouse model was characterized by analyzing their phenotypic features, weight trends, NMJ abnormalities and cell death transcripts. Due to an early up-regulation of transcripts involved in cell death, these mice were to be treated with Pifithrin-α, a drug that inhibits P53, and qRT-PCR was to be used to assess the impact on the cell death transcripts in the spinal cord.

Chapter 2: Methods

Mouse Maintenance

The SMA mouse models used include the intermediate model, $Smn^{2B/-}$, and the severe model, $Smn^{-/-}$;$SMN2^{(tg/0)}$. $Smn^{2B/-}$ mice were established in our laboratory (please see results for establishment of colony, Figure 14). $Smn^{2B/+}$ mice (imported from the Kothary Laboratory, University of Ottawa) were interbred with wild type C57Bl6J mice to produce $Smn^{2B/+}$ mice for subsequent breeding. $Smn^{+/-}$ mice were kindly provided by Prof Tom Gillingwater. $Smn^{2B/+}$ and $Smn^{+/-}$ mice were interbred to produce $Smn^{2B/-}$ mice alongside littermates ($Smn^{+/+}$; $Smn^{+/-}$; $Smn^{2B/+}$) all of which were phenotypically normal. Wild type littermates ($Smn^{+/+}$) were used as controls. These breeding pairs were maintained at the University of Edinburgh animal facilities in IVC caging. $Smn^{-/-}$; $SMN2^{(tg/0)}$ mice were kindly provided by Prof Tom Gillingwater. Breeding pairs of $Smn^{-/-}$;$SMN2^{(tg/tg)}$ and $Smn^{+/-}$;$SMN2^{(0/0)}$ mice were again maintained at the University of Edinburgh animal facilities. Heterozygous littermates ($Smn^{+/-}$;$SMN2^{(tg/0)}$) were used as controls.

All mice were sacrificed by an overdose of anaesthetic (IsoFlo, Abbott, Québec, Canada). All procedures were carried out in accordance with the procedures approved and licenced by the Home Office, United Kingdom. Mice for qRT-PCR analysis were sacrificed at a pre-symptomatic time point (P10 for $Smn^{2B/-}$ mice, P2 for $Smn^{+/-}$;$SMN2^{(tg/0)}$). At these ages, SMA models have no apparent phenotypic features of the disease and are approximately the same weight and have a similar righting time as littermates. Wild type mice were sacrificed at P10, the age at which the $Smn^{2B/-}$ mice are pre-symptomatic. The re-derived $Smn^{2B/-}$ mice were sacrificed at P7, pre-symptomatic, and P20, late symptomatic.

PCR for Genotyping

DNA was extracted from tail tips by digesting the tissue in TTLB (Tail Tip Lysis Buffer; 0.5M EDTA, 1M Triz-HCL, 1M NaCL, 10% SDS, ddH2O) and Proteinase K

(1mg/ml) overnight at 55°C. DNA was precipitated in 500 μl isopropanol and washed in ethanol before suspending in 200 μl of distilled water to give a concentration of approximately 200ng/μl.

To establish which mice carried the *Smn2B* allele, PCR was preformed using the Invitrogen Taq polymerase kit and a forward (5'-AACTCCGGGTCCTCCTTCCT-3') and reverse (5'-TTTGGCAGACTTTAGCAGGGC-3') primer. The following temperature cycling protocol was used:

Step 1:	94°C for 3 minutes
Step 2:	94°C for 45 seconds
Step 3:	58°C for 45 seconds
Step 4:	72°C for 45 seconds
Repeat cycles 2-4 35 times	
Step 5:	72°C for 5 minutes
Hold at 4°C	

To distinguish $Smn^{+/-}$ from $Smn^{+/+}$ mice, PCR was preformed using the GoTaq Flexi DNA polymerase kit, a forward primer (5'-ATAACACCACTCTTACTC-3') and two reverse primers (5'-GTAGCCGTGATGCCATTGTCA-3'; 5'-AGCCTGAAGAACGAGATCAGC-3'). The following temperature cycling protocol was used:

Step 1:	94°C for 2 minutes
Step 2:	94°C for 30 seconds
Step 3:	58°C for 30 seconds
Step 4:	68°C for 1 minute
Repeat cycles 1-4 35 times	
Step 5:	72°C for 5 minutes
Hold at 8°C	

Subsequently, gel electrophoresis separated DNA fragments and allowed the visualisation of the various genotypes (Please see Figure 15 in results for genotyping outcomes). DNA was run on a 1% agarose gel in 1X TAE at 100V for 40 minutes.

qRT-PCR

The whole spinal cord of recently sacrificed mice were removed, snap frozen on dry ice and stored at -80^{o}C. RNA was extracted using a micro RNeasy kit (Qiagen), according to manufacturers instructions. Subsequently, 1ug of RNA was used to perform reverse transcriptase using the RT^{2} First Strand kit (Qiagen), as per manufacturers instructions. SYBR green-based qRT-PCR was preformed using Kapa SYBR Fast Universal (Kapa Biosystems, KK4602) and the CFX Connect Real-time PCR Detection system (Biorad). Custom-made primers (Sigma) were optimised before use (please see Figure 2 in results section) and pre-optimised primers were purchased from Biorad. Two housekeeping genes were used in each reaction (a combination of *β-Actin*, *GAPDH*, *PPIA* and *Y-whaz*) and all samples were run in technical triplicate.

Immunofluorescence

Spinal cord and brainstems, removed from recently sacrificed mice were fixed in 4% Paraformaldehyde (PFA; Electron Microscopy Science) in PBS overnight and washed in Phosphate Buffered Saline (PBS) the following day. They were immersed in 30% sucrose overnight and embedded in 50% OCT compound, 15% sucrose in PBS. The embedded tissue was frozen on dry ice and stored at -80^{o}C. Frozen sections were cut at 12μm on a cryostat (Leica) and stored at -20^{o}C on glass slides. Staining was done in the Sequenza Immunostaining Centre (Fisher). Sections were washed in PBS, permeabilised in 0.3% Triton X-100 in PBS for 10 minutes and blocked in 4% BSA, 0.3% Triton in PBS for 30 minutes. They were then incubated in a primary antibody (rabbit anti-53BP1, Cambridge Bioscience; rabbit anti-pH2AX, Cell Signaling Technology) in blocking solution at 4^{o}C overnight at a dilution of 1:250. The secondary antibody (AlexaFluor 555 Goat anti-Rabbit, Life Technologies) was applied for 2 hours at 1:200. Sections were stained with the fluorescent Nissl stain NeuroTrace 500/525 (Life Technologies) at 1:50 for 30 minutes and DAPI (Life Technologies) at 1:1000 for 5 minutes before mounting in Mowiol (Sigma). Images of motor neurons within the thoracic region of the spinal

cord and within the facial nuclei of the brainstem were captured on a confocal microscope (Nikon A1R FLIM) at a 40x magnification.

For neuromuscular junction (NMJ) labelling, muscles were removed from recently sacrificed mice and fixed in 4% PFA (Electron Microscopy Science) in PBS for 15 minutes. Muscles were permeabilised in 2% Triton X-100 for 30 minutes and blocked in 4% BSA, 1% Triton for 30 minutes before incubation in primary antibodies (Neurofilament (2H3) and Synaptic vesicle protein 2 (SV2), both at 1:50, Developmental Studies Hybridoma Bank) at 4^{o}C on a rocking platform for 4 days. Following two 10 minute PBS washes, muscle were immersed in α-Bungarotoxin at 1:200 for 2 hours to label Post-synaptic Acetylcholine receptors and subsequently the secondary antibody (Cyc3 Goat anti-Mouse, Jackson) at 1:250 overnight. Muscles were washed in PBS and mounted in Mowiol (Sigma). NMJs were imaged on a confocal microscope (Ziess Axioskop) and a Z-stack produced at 40x magnification.

Image Analysis

Fiji Image Processing Software was used to analyse images of motor neurons. Images were blinded to ensure there was no knowledge of whether the image was from brainstem or spinal cord sections. All analysis was carried out in grayscale. Motor neurons were distinguished from other neuronal material by their large size and irregular shape. Only motor neurons that conformed to this criterion and had a visible nucleus were analysed. The maximum staining intensity for P53BP and pH2AX was measured by tracing the periphery of each motor neuron and instructing the software to measure the mean grey value of the area within.

Microsoft Excel (Mac 2011) was used to collate the measurement information and this was subsequently analysed in GraphPad Prism (Version 6 for Mac OS X). All graphs were produced in GraphPad Prism.

Injection with Pifithrin-α

A 20mg/ml Pifithrin-α and DMSO (Dimethyl Sulfoxide) solution was diluted to 0.6mg/ml in Saline. Mice were injected with 2mg/kg of the solution via intraperitoneal injection daily from P5–P9. Untreated mice received a daily injection of 0.6mg/ml solution of DMSO only. Treated and untreated mice were sacrificed 1 hour after the final injection and spinal cords were immediately removed. These were snap frozen and stored at -80^{o}C.

Chapter 3: Investigating transcriptional differences between differentially vulnerable motor neurons

Introduction

SMA is caused by a mutation or deletion of the *SMN1* gene, which results in a reduction of SMN protein.[3,4] The exact function of this ubiquitously expressed protein is currently unknown however, there are various suggested functions of SMN.

SMN is known to be involved in pre-mRNA splicing, which is a process whereby non-coding introns are removed from pre-mRNA and the exons are rejoined to allow translation to progress.[24] This is facilitated by the spliceosome, which consists of a variety of components. One of the components is snRNPs (small nuclear ribonuclear proteins) and, *in vivo*, SMN is important in the assembly of these. In this role, Smn exists as a complex that comprises of SMN and several Gemin proteins, Gemin 2-7.[25] The SMN complex can then bind Sm proteins and together with snRNAs (small nuclear RNAs) they create snRNPs.[25] There are both major and minor spliceosomes. These differ in their composition of snRNAs and minor spliceosomes are thought to be responsible for splicing only ~1% of transcripts.[26,27] However, minor splicosomes are more affected by a reduction in SMN and therefore, although there may only be a small number of splicing defects, these may affect RNAs that are particularly important in motor neurons.[26,28] Thus explaining the selective vulnerability of motor neurons.

However, it has been suggested that SMN's role in splicing is not the causative factor of the SMA phenotype and instead splicing defects are a consequence of the disease.[29] This is since the majority of splicing products are similar in SMA mouse models and wild type mice until later on in the disease progression.[29] Therefore, other functions of SMN that, when disrupted, could cause SMA have been suggested. For example, roles in axonal transport of RNA or in actin dynamics have been proposed.[30,31]

Although it is clear that a reduction in SMN disrupts many cellular processes, it is still not clear which of these disrupted processes contributes to the degeneration of motor neurons. It is also not clear why not all motor neurons degenerate and some appear to be resistant to degeneration. This phenomenon is observed in both patients and SMA mouse models.[32,9] SMA patients experience progressive paralysis in the muscles of their trunk and limbs due to denervation, however proximal limb muscles are more affected than distal muscles.[32] In addition, the diaphragm and facial muscles remain innervated, with facial weakness being seen in only very severe cases.[32] In Amyotrophic Lateral Sclerosis (ALS), another type of Motor Neuron Disease, this is also seen as eye movements are preserved in severe ALS patients.[33] SMA mouse models also display this differential vulnerability of motor neurons. In the severe mouse models of SMA, abnormal NMJs and denervation is visible in abdominal muscles whilst specific cranial muscles (the rostral band of the Levator Auris Longus and Adductor Auris Longus muscles[34]) lack these features, even late on in the disease progression.[9,13] This differential vulnerability between abdominal and cranial muscles is even more distinct in the intermediate *Smn*$^{2B/-}$ mouse model of SMA.[20,35]

In the work by Murray *et. al.* (Acta Neuropathol. Commun., *In Press*), that was described in the introduction to this thesis, transcriptional profiles of differentially vulnerable motor neurons in the *Smn*$^{2B/-}$ mouse model of SMA and wild type mice were compared. By filtering for transcriptional changes that occurred in the comparison of *Smn*$^{2B/-}$ and wild type vulnerable motor neurons and in the comparison of *Smn*$^{2B/-}$ and wild type resistant motor neurons, transcriptional changes that correlated with a reduction in SMN could be highlighted (Figure 1; blue arrows). This provided an insight into the pathways that are disrupted by a reduction in SMN. They noted that transcripts involved in rRNA binding and in ubiquitination were down-regulated in both *Smn*$^{2B/-}$ vulnerable and resistant motor neurons compared to their wild type counterparts. In addition, transcripts involved in cell death pathways were up-regulated in vulnerable motor neurons of the *Smn*$^{2B/-}$ mouse compared to their counterparts in wild type mice. Although this up-regulation in cell death transcripts did not appear in the comparison of resistant motor neurons of *Smn*$^{2B/-}$ and

wild type mice, it was of particular interest due to the pre-symptomatic time point at which this up-regulation was observed.

Murray *et. al.* also looked for changes that occurred between vulnerable and resistant motor neurons. This was done by comparing vulnerable *Smn*$^{2B/-}$ motor neurons to resistant *Smn*$^{2B/-}$ motor neurons and to wild type vulnerable motor neurons (Figure 1; red arrows). They noted that transcripts involved in DNA repair were up regulated in resistant motor neurons compared with vulnerable motor neurons suggesting that this provides them with some level of protection (Figure 1; red arrows). The transcriptional changes that occurred between these motor neurons could provide an insight into why some motor neurons are resistant to degeneration and others are not.

In this chapter, I aimed to detect transcriptional changes that were identified by RNAseq by either qRT-PCR or immunofluorescence. Firstly, transcripts that are altered by a reduction in SMN were investigated. I aimed to detect the changes in transcripts implicated in rRNA binding, ubiquitination and cell death in whole spinal cord cDNA using qRT-PCR. Based on the result from the RNAseq screen, we hypothesized that we would detect changes in transcripts involved in these cellular processes. Although changes in transcripts involved in ubiquitination and cell death between wild type and *Smn*$^{2B/-}$ mice were detectable by qRT-PCR, changes in transcripts involved in rRNA binding could not be detected. Secondly, transcripts that may provide motor neurons with resistance against degeneration were investigated. I aimed to detect alterations in DNA repair between vulnerable and resistant motor neurons using immunofluorescence against protein markers of DNA repair. The intensity of fluorescence staining was quantified to provide an indication of the level of DNA repair taking place in different motor neurons. Based on the results of the RNAseq screen, we hypothesized that motor neurons in the brainstem would have an increased intensity of staining for these DNA repair markers. Following analysis of staining, there was no significant difference between the staining intensity of brainstem motor neurons compared with spinal cord motor neurons.

Results

Firstly, transcripts identified by RNAseq as being altered by a reduction in SMN were investigated. Using qRT-PCR transcripts in the whole spinal cord of *Smn*$^{2B/-}$ mice and wild type mice were compared. In order to investigate whether transcriptional changes can be detected by qRT-PCR, primer sets specific for transcripts being investigated were sourced. A variety of pre-optimized and custom-made primers were used. Custom made primers had to be optimized before use to establish whether they were specific and quantitative. Where primers were deemed not suitable, due to not having the correct efficacy or product size (see below), pre-optimized primers were purchased. Figure 2 displays the process of optimization carried out for primers, using the housekeeping gene *PPIA* as an example. To identify the optimal annealing temperature, we performed a gradient qRT-PCR in which the annealing temperature was varied. In this example, primers were directed against *PPIA* and cDNA samples were exposed to 8 different annealing temperatures ranging from 55^{o}C to 65^{o}C (Figure 2A). The curve that has the lowest Ct (cycle threshold) value and therefore crosses the threshold first, corresponds to the sample that was exposed to the optimum temperature for a given primer set. For PPIA this temperature was 64.5^{o}C. This is the temperature at which the greatest volume of *PPIA* product is generated in the fewest cycles and therefore is the annealing temperature that will be used for all subsequent qRT-PCR experiments involving this primer set. In order to assess the efficiency of the primers directed against *PPIA*, a standard curve was created. A standard curve plots the log of the starting volume of cDNA against the Cq (quantitation cycle) value, which is reflective of the level of fluorescence detected (Figure 2B). To produce varying log values a dilution series of cDNA, of which the concentrations of cDNA are known, was set up. The standard curve is a linear graph and its gradient will determine the efficacy of the primer set. The efficacy of the primer should lie between 90-110% and therefore, with the value of 94.5%, *PPIA* primers have an appropriate efficiency for future use. In order to confirm that the product produced was the desired target, the size of the amplified product was determined. Gel electrophoresis revealed the length of the product of *PPIA* was 150 base pairs (Figure 2C). This was the expected length of the product,

due to the distance between the binding sites of the forward and reverse *PPIA* primers. Together this analysis shows that these primers have an optimal annealing temperature of 64.5°C, have an efficiency within the desired limits and produce a produce of expected size. Based on this data, these *PPIA* primers were deemed appropriate for use in quantitative experiments. The same procedures were repeated for all primer sets used.

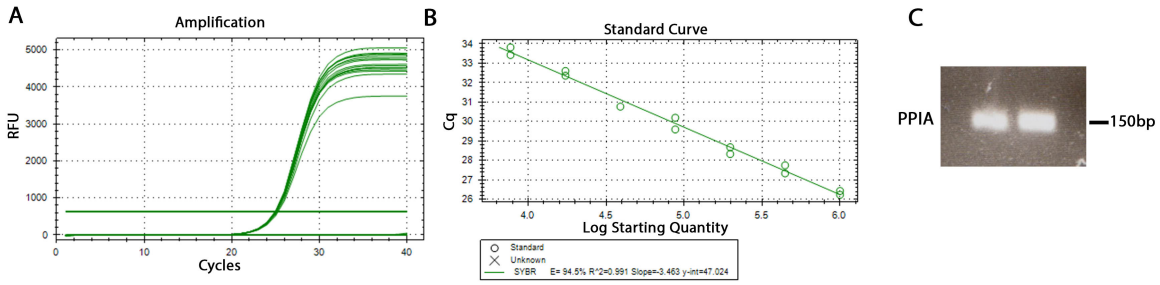

Figure 2: Custom-made primer sets were optimized before use. Here, the optimization of *PPIA* acts as an example to show the protocol used to optimize all custom-made primer sets. (A) The curves on this graph are created by plotting the fluorescence intensity of samples against the number of amplification cycles. Samples had the same starting volume of cDNA but were exposed to various annealing temperatures. The curve that crosses the horizontal, threshold line first denotes the sample exposed to the optimum annealing temperature. For *PPIA*, this was 64.5°C (RFU = relative fluorescence units). (B) A standard curve is created by plotting the fluorescence intensity against the log of the starting quantity of cDNA. A dilution series of cDNA (dilution factor = 1:5) creates varying starting concentrations. These are exposed to the optimal annealing temperature for PPIA. The standard curve reveals the efficacy of the primer set. An efficacy between 90-110% is desirable. *PPIA* had an efficacy of 94.5% (quantitation cycle). (C) The product length of *PPIA* was as expected, approximately 150bp.

Following optimization, suitable primers were used to investigate, by qRT-PCR, transcriptional changes that correlated with reduced SMN levels. Whole spinal cord cDNA of P10 (pre-symptomatic) *Smn*$^{2B/-}$ and wild type mice was used rather than the cDNA derived from laser captured (LCM) motor neuron cell bodies that was used by Murray e*t. al.* (Acta Neuropathol. Commun., *In Press*). The level of some transcripts in LCM cDNA samples is too low to be detected by qRT-PCR and amplification of the cDNA samples to increase the levels of these transcripts introduced qRT-PCR inhibitors that interfered with the qRT-PCR reaction. Whole spinal cord cDNA can be used in this situation as the comparison of distinct motor neuron pools is not

necessary to detect transcriptional changes that correlate with SMN reduction, rather the comparison of spinal cord tissue is sufficient.

One of the top functional clusters that was identified during the previous RNAseq screen was 'ribosome and rRNA binding proteins'. Transcripts, including *MRPL20* (mitochondrial ribosomal protein L20) and *RPS27A* (ribosomal protein S27a), were previously shown to be down-regulated in cell bodies of $Smn^{2B/-}$ mice compared with wild type.[15] Since *MRPL20* and *RPS27A* had a relatively high fold change in regulation, they were used to investigate whether transcriptional changes can be detected by qRT-PCR. qRT-PCR showed there was no significant difference between the transcript levels of both *MRPL20* and *RPS27A* in $Smn^{2B/-}$ mice compared to wild type mice (Figure 3). This result implies that either the change in transcript levels are too small to be detected by qRT-PCR on whole spinal cord cDNA or that this change, which was detected by RNAseq, is not consistent in new biological replicates.

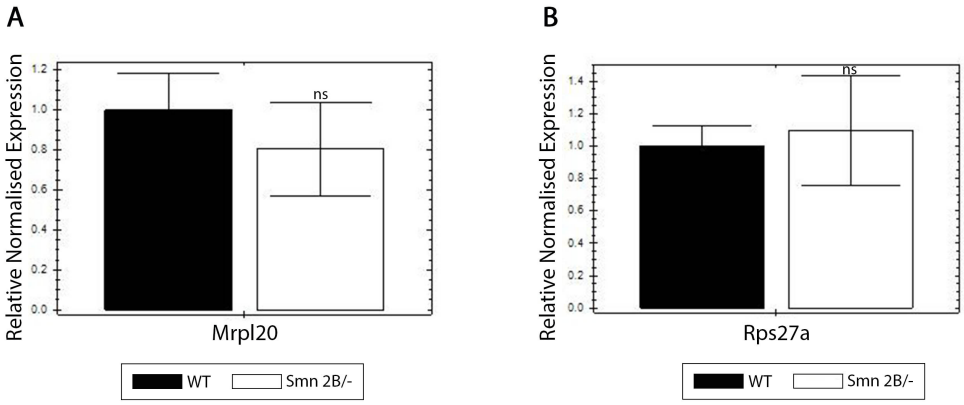

Figure 3: There is no change in transcripts associated with rRNA binding in $Smn^{2B/-}$ mice at a pre-symptomatic stage. qRT-PCR analysis was used to compare the transcript levels of *MRPL20* and *RPS27A* in cDNA from $Smn^{2B/-}$ and control (WT) mice at P10 (pre-symptomatic). (A) Bar chart (Mean ± SEM) shows that the relative normalized expression of *MRPL20* is not significantly changed in $Smn^{2B/-}$ mice compared to controls at P10 (B) Bar chart (Mean ± SEM) shows that the relative normalized expression of *RPS27A* is not significantly changed in $Smn^{2B/-}$ mice compared to controls at P10 (By Mann Whitney U Test; n=4 mice per genotype).

Murray *et. al.* (Acta Neuropathol. Commun., *In Press*) also showed that the ubiquitination pathway was down-regulated in the $Smn^{2B/-}$ mouse model. We therefore investigated the transcript levels of Ubiquitin (*UBB*) by qRT-PCR. This

showed that *UBB* was significantly down-regulated in the *Smn*$^{2B/-}$ mouse model compared to wild type mice (Figure 4) and therefore is in agreement with the RNAseq results. This suggests that the functional cluster of ubiquitination is down-regulated in the *Smn*$^{2B/-}$ mouse model of SMA and therefore may be involved in SMA. This is consistent with previous reports describing defects in ubiquitination in SMA models.[36]

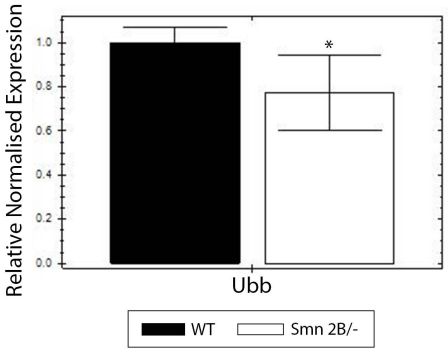

Figure 4: There is a down-regulation of Ubiquitin in Smn$^{2B/-}$ mice at a pre-symptomatic stage. qRT-PCR analysis was used to compare the transcript levels of Ubiquitin (*UBB*) in cDNA from *Smn*$^{2B/-}$ and control (WT) mice at P10 (pre-symptomatic). Bar chart (Mean ± SEM) shows that the relative normalized expression of *UBB* is significantly down regulated in *Smn*$^{2B/-}$ mice compared to wild type controls at P10 (*P<0.05 by Mann Whitney U Test; n=4 mice per genotype).

Furthermore, the RNAseq by Murray *et. al*. (Acta Neuropathol. Commun., *In Press*) showed an up-regulation of transcripts involved in cell death, specifically the P53 signaling pathway. *FAS*, *CDKN1A* (Cyclin-Dependant Kinase Inhibitor 1A) and *PMAIP1* (Phorbol-12-Myristate-13-Acetate-Induced Protein 1) are all involved in this signaling pathway and again they all showed a high fold change between *Smn*$^{2B/-}$ and wild type mice. Therefore, they were investigated by qRT-PCR. This revealed that all three transcripts were significantly up-regulated in the *Smn*$^{2B/-}$ mouse compared to wild type mice (Figure 5). As above the up-regulation of these transcripts in the *Smn*$^{2B/-}$ mouse model may suggest that pathways involved in cell death may be up-regulated at pre-symptomatic stages in SMA models.

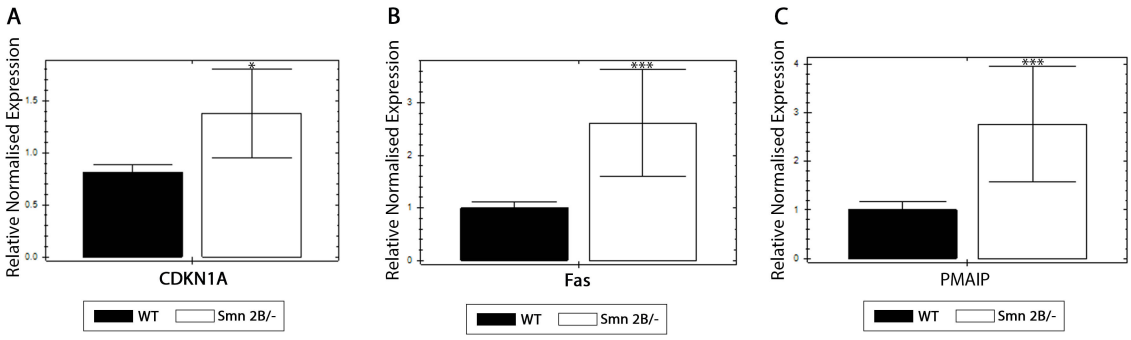

Figure 5: There is an up-regulation of transcripts involved in cell death in Smn$^{2B/-}$ mice at a pre-symptomatic stage. qRT-PCR analysis was used to compare the transcript levels of *CDKN1A*, *FAS* and *PMAIP1* in cDNA from *Smn*$^{2B/-}$ and control (WT) mice at P10 (pre-symptomatic). Bar charts (Mean ± SEM) show that the relative normalized expression of *CDKN1A* (A), *FAS* (B) and *PMAIP1* (C) are all significantly up-regulated in *Smn*$^{2B/-}$ mice compared to wild type controls at P10 (*P<0.05, ***P<0.001 by Mann Whitney U Test; n=4 mice per genotype).

The data above demonstrates that some transcriptional changes can be detected by qRT-PCR. Therefore, the changes that were detectable were further investigated in the more severe *Smn*$^{-/-}$;*SMN2*$^{(tg/0)}$ mouse model of SMA. This would clarify whether these changes are exclusive to the *Smn*$^{2B/-}$ model or whether they appear to be universal in SMA mouse models. Whole spinal cord cDNA of pre-symptomatic (P2) *Smn*$^{-/-}$;*SMN2*$^{(tg/0)}$ mice and control littermates was used for analysis. It was observed that *UBB* was significantly down-regulated in the *Smn*$^{-/-}$;*SMN2*$^{(tg/0)}$ mouse model compared to controls (Figure 6). Additionally, even though *CDKN1A* was not significantly different between *Smn*$^{-/-}$;*SMN2*$^{(tg/0)}$ mice and controls, *FAS* and *PMAIP1* were significantly up-regulated in this severe SMA mouse model (Figure 7).

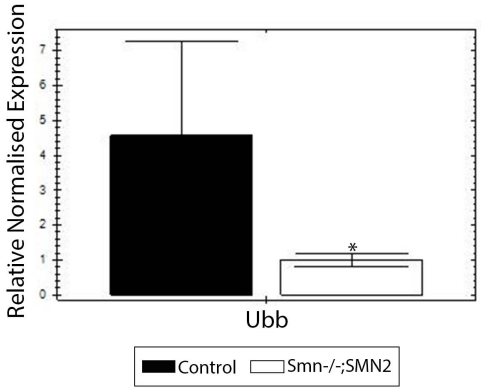

Figure 6: There is a down-regulation of Ubiquitin in *Smn*$^{-/-}$;*SMN2*$^{(tg/0)}$ mice at a pre-symptomatic stage. qRT-PCR analysis was used to compare the transcript levels of *UBB* in cDNA from *Smn*$^{-/-}$;*SMN2*$^{(tg/0)}$ and control (*Smn*$^{+/+}$;*SMN2*$^{(tg/0)}$) mice at P2 (pre-symptomatic). Bar chart (Mean ± SEM) shows that the relative normalized expression of *UBB* is significantly down regulated in *Smn*$^{-/-}$;*SMN2* mice compared to controls (*P<0.05 by Mann Whitney U Test; n=3 mice per genotype).

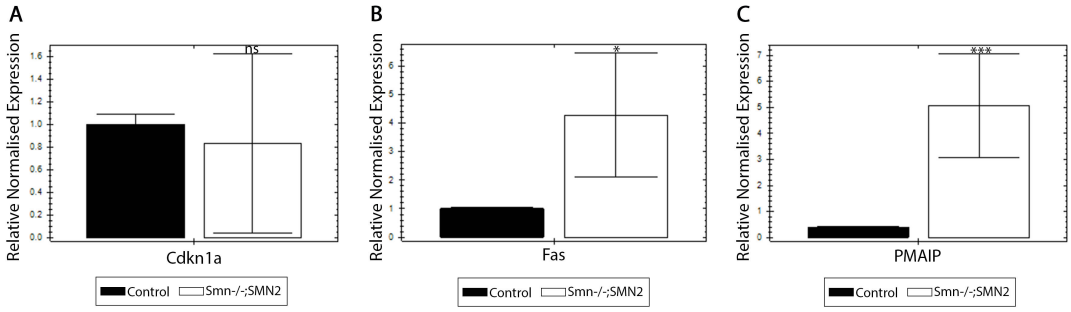

Figure 7: There is an up-regulation of transcripts involved in cell death in *Smn$^{-/-}$;SMN2$^{(tg/0)}$* mice at a pre-symptomatic stage. qRT-PCR analysis was used to compare the transcript levels of *CDKN1A*, *FAS* and *PMAIP1* in spinal cord cDNA from *Smn$^{-/-}$;SMN2$^{(tg/0)}$* and control (*Smn$^{+/+}$;SMN2$^{(tg/0)}$*) mice at P2 (pre-symptomatic). (A) Bar chart (Mean ± SEM) shows that the relative normalized expression *CDKN1A* was not significantly altered in *Smn$^{-/-}$;SMN2$^{(tg/0)}$* mice. Bar charts (Mean ± SEM) for *FAS* (B) and *PMAIP1* (C) show that the relative normalized expression of these transcripts are both significantly up regulated in *Smn$^{-/-}$;SMN2$^{(tg/0)}$* mice compared to controls at P2 (*P<0.05 by Mann Whitney U Test; n=3 mice per genotype).

Secondly, transcripts that may provide motor neurons with resistance against degeneration were investigated. DNA repair was highlighted, by Murray *et. al.* (Acta Neuropathol. Commun., *In Press*), as a functional cluster that could provide resistance to degeneration as there was a greater level of transcripts involved in DNA repair in resistant motor neurons compared to vulnerable motor neurons. Further investigation into DNA repair was carried out using immunofluorescence rather than qRT-PCR as resistant and vulnerable motor neuron pools are within the same mouse. As they are in different regions of the mouse and these regions, the brainstem and spinal cord, contain a different concentration of motor neurons, performing qRT-PCR on the whole tissues would not give an accurate representation of transcriptional differences within the motor neurons. Previous attempts have been made to perform qRT-PCR on transcripts involved in DNA repair on laser captured motor neurons. However, the relative abundance of these transcripts made this technically extremely challenging. Instead, brainstem and spinal cord sections were stained for markers of DNA repair by immunofluorescence. Markers of DNA repair include pH2AX (phosphorylated Histone H2A family member X) and P53BP (P53 Binding Protein).

H2AX is phosphorylated (creating pH2AX) at sites of DNA damage early after damage has occurred to attract other important factors to the site in order to facilitate DNA repair.[37] It can therefore provide information about the amount of DNA repair occurring.[38] Motor neurons of the brainstem and spinal cord were stained for pH2AX and were counterstained with florescent Nissl and DAPI (Figure 10A). They were imaged on a confocal microscope and captured images were analysed in Fiji Imaging Software. Since images of pH2AX, Nissl and DAPI staining of each motor neuron could be separated, tracing of motor neurons could be carried out using Nissl staining as a guide on one channel and the intensity of pH2AX staining could be measured on another channel. The intensity is measured as mean grey value. A greater mean grey value indicates a greater level of protein. Mean grey values from motor neurons in the spinal cord and brainstem were collated. An unpaired T-test of the mean grey values of motor neurons in the spinal cord and brainstem showed there was no statistically significant difference in intensity between these two motor neuron populations (Figure 10B). In order to investigate whether there was significant inter-mouse variability in the levels of DNA repair that could mask potential differences between neuronal populations, the average of the mean grey values for the spinal cord and brainstem of each mouse was subjected to a paired T-test. This was also not statistically different (Figure 10C).

pH2AX can also be assessed by counting bright foci within the nucleus of cells.[38] However, bright foci were difficult to count in the staining produced here therefore, the intensity of staining within each motor neuron was categorised into 'negative' (no staining apparent), 'faint', or 'bright'. Once collated each category was subjected to a paired t-test to compare, for example, the amount of faintly stained motor neurons in the spinal cord to the amount of faintly stained motor neurons in the brainstem. There was no significant difference in negative, faint or bright staining of pH2AX between the brainstem and spinal cord (Figure 10D). Overall, the results suggest that pH2AX is not altered between motor neurons of the spinal cord and brainstem.

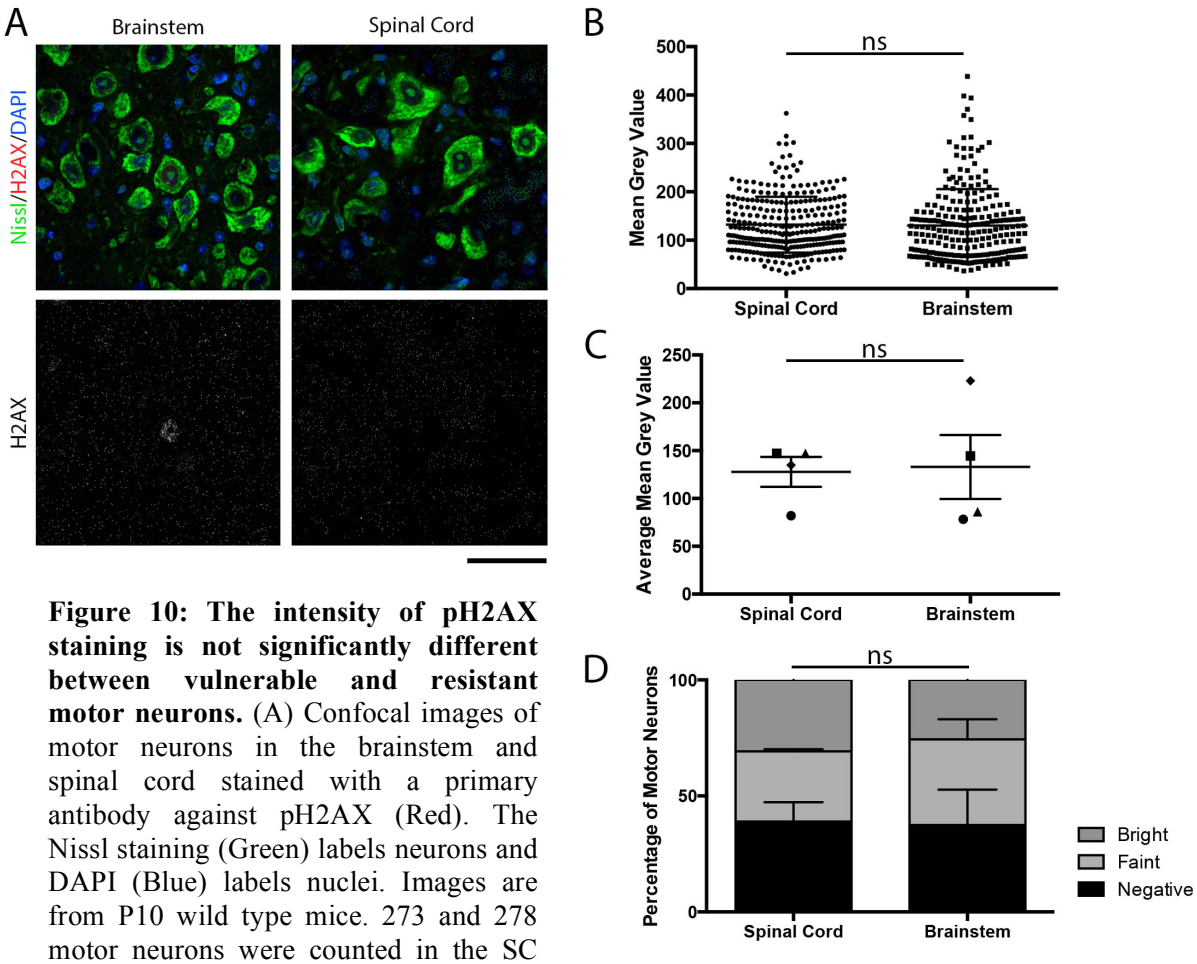

Figure 10: The intensity of pH2AX staining is not significantly different between vulnerable and resistant motor neurons. (A) Confocal images of motor neurons in the brainstem and spinal cord stained with a primary antibody against pH2AX (Red). The Nissl staining (Green) labels neurons and DAPI (Blue) labels nuclei. Images are from P10 wild type mice. 273 and 278 motor neurons were counted in the SC and BS respectively (Scale Bar = 50μm). of pH2AX staining in motor neurons of the spinal cord and brainstem. There is no significant difference. (C) The average of the mean grey value for the spinal cord and brainstem of each mouse is plotted on the graph (Mean±SEM). The different symbols represent different mice. There is no significant difference between the staining in motor neurons of the spinal cord and brainstem (D) The intensity of pH2AX staining within motor neurons was rated as negative (if there was no staining), faint or bright. The bar chart collates these results showing the percentage of each category in the brainstem and spinal cord (Mean±SEM). There was no significant difference between negative, faint or bright staining of pH2AX between the brainstem and spinal cord (n= 4 mice).

P53BP also appears early at sites of DNA repair following DNA damage and mice that are deficient in this protein are unable to elicit normal DNA repair mechanisms.[39,40] Therefore, P53BP can serve as another marker of DNA repair and the methods used to analyse pH2AX were repeated for P53BP. Motor neurons of the brainstem and spinal cord were stained for P53BP and were counterstained with florescent Nissl and DAPI (Figure 11A). Mean grey values of P53BP staining in motor neurons were collated. An unpaired T-test of the mean grey values of P53BP staining in motor neurons of the spinal cord and brainstem showed there was no

statistically significant difference (Figure 11B). Again, to account for inter-mouse variability the average of the mean grey values for the spinal cord and brainstem of each mouse was subjected to a paired T-test. This was also not statistically different (Figure 11C). In keeping with the methods used for pH2AX, the intensity of P53BP was categorized into 'negative' (no staining apparent), 'faint', or 'bright'. There was also no significant difference in negative, faint or bright staining of P53BP between the brainstem and spinal cord of each wild type mouse.

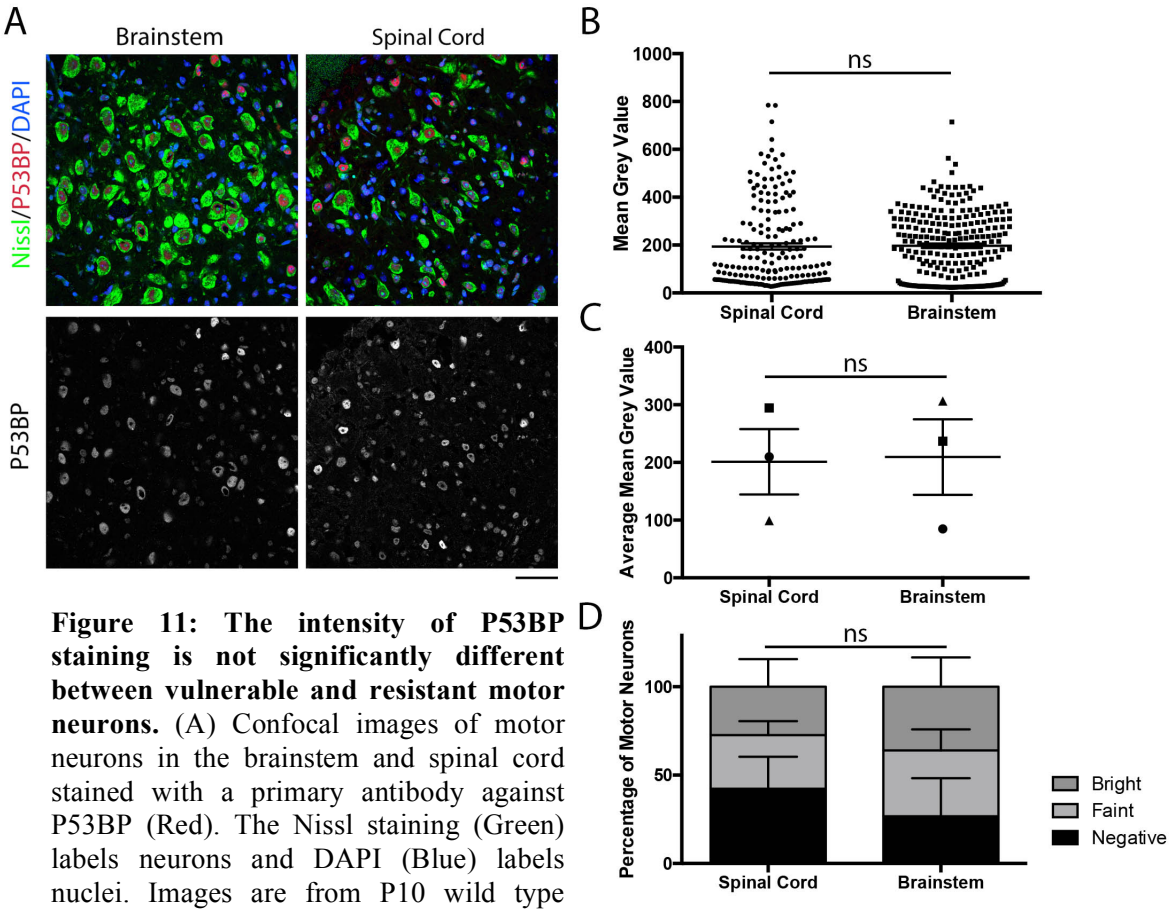

Figure 11: The intensity of P53BP staining is not significantly different between vulnerable and resistant motor neurons. (A) Confocal images of motor neurons in the brainstem and spinal cord stained with a primary antibody against P53BP (Red). The Nissl staining (Green) labels neurons and DAPI (Blue) labels nuclei. Images are from P10 wild type mice. 190 and 200 motor neurons were counted in the SC and BS respectively (Scale Bar = 50μm).
(B) The scatterplot (Mean ± SEM) displays the mean grey values of P53BP staining in motor neurons of the spinal cord and brainstem. There is no significant difference. (C) The average of the mean grey value for the spinal cord and brainstem of each mouse is plotted on the graph (Mean±SEM). The different symbols represent a different mouse. There is no significant difference between the staining in motor neurons of the spinal cord and brainstem (D) The intensity of P53BP staining within motor neurons was rated as negative (if there was no staining), faint or bright. The bar chart collates these results showing the percentage of each category in the brainstem and spinal cord (Mean± SEM). There was no significant difference between negative, faint or bright staining of P53BP between the brainstem and spinal cord (n= 3 mice).

Discussion

Firstly, transcriptional changes that correlate with a reduction in SMN were investigated in pre-symptomatic *Smn*$^{2B/-}$ and wild type mice, using qRT-PCR. A change in transcripts associated with ribosomal proteins between wild type and *Smn*$^{2B/-}$ mice could not be detected. However, qRT-PCR showed a down-regulation of ubiquitin transcript, involved in ubiquitination, and an up-regulation of transcripts involved in cell death in the *Smn*$^{2B/-}$ mouse model of SMA. These detectable changes were also shown to occur, by qRT-PCR, in pre-symptomatic *Smn*$^{-/-}$;*SMN2*$^{(tg/0)}$ mice, a more severe mouse model of SMA. Secondly, DNA repair activity in differentially vulnerable motor neurons was investigated. There was shown to be no significant difference in DNA repair activity between resistant, brainstem motor neurons and vulnerable spinal cord motor neurons.

Some transcriptional changes that had been noted to occur between wild type and SMA mice from previous RNAseq analysis, carried out by Murray *et. al*. (Acta Neuropathol. Commun., *In Press*), could not be detected by qRT-PCR. The previous RNAseq analysis was preformed on motor neuron cell bodies, obtained by LCM, not on whole spinal cord cDNA, perhaps explaining the obtained results. As stated earlier, LCM cDNA could not be used as the level of some transcripts in LCM cDNA samples is too low to be detected by qRT-PCR. Amplification of LCM cDNA samples to increase the levels of these transcripts introduced qRT-PCR inhibitors that interfered with the qRT-PCR reaction. Whole spinal cord cDNA could be used as the comparison of distinct motor neuron pools was not necessary to detect transcriptional changes that correlate with SMN reduction, rather the comparison of whole spinal cord tissue from a wild type mouse and a SMA mouse model is sufficient. However, motor neuron cell bodies make up a relatively small proportion of the entire spinal cord and the abundance of other cell types may mask the small transcriptional changes occurring in motor neurons.

Transcripts associated with rRNA binding proteins, including *MRPL20* and *RPS27A*, were not significantly altered in the qRT-PCR analysis. rRNA binding proteins are

ribosomal proteins that along with rRNA create the ribosomal subunit that is responsible for translation. Disruptions in translation have been linked to Spinal Muscular Atrophy with Respiratory Distress (SMARD), a disorder caused by mutations of the protein IGHMBP2 rather than SMN.[41,42] Therefore, due to the importance of ribosomal proteins in translation, the down-regulation observed in the previous RNAseq results should not be over-looked. Therefore in the future, it may be interesting to investigate rRNA binding proteins themselves, perhaps by western blotting to provide quantification of the concentration of these proteins in the spinal cords of wild type and SMA mouse models.

Ubiquitin (*UBB*) transcript was down-regulated in both the $Smn^{2B/-}$ and the $Smn^{-/-};SMN2^{(tg/0)}$ mouse models of SMA. Ubiquitination involves the addition of ubiquitin to proteins to mark them for degradation.[43] Perhaps the malfunction of this pathway may lead to the build up of proteins that should be degraded and in motor neurons they may disrupt the normal homeostasis, creating a toxic like effect. Wishart *et. al.* (2014) demonstrated that there is a build up of beta-catenin, a down-stream target of the ubiquitinaton pathway, in distal axons of SMA models and that inhibiting this pharmacologically can modify the SMA phenotype.[36]

Transcripts involved in cell death, specifically the P53 signaling pathway, were significantly up-regulated in both the $Smn^{2B/-}$ and the $Smn^{-/-};SMN2^{(tg/0)}$ mouse models of SMA. It should be noted that this up-regulation in the cell body of motor neurons was at a pre-symptomatic time point, before any NMJ pathology is noticeable. It is not known whether the death of motor neurons in SMA is caused by defects at the NMJ inducing cell death or whether nuclear defects are to blame, with the NMJ simply being the most vulnerable part of the cell and therefore the first part with visible deformities.[44] The confirmation that markers of cell death are up-regulated in two mouse models of SMA, pre-symptomatically, would support the latter belief. Furthermore, it has been shown that full length SMN protein has an anti-apoptotic effect while SMNΔ7 does not and in fact SMNΔ7 increases apoptosis.[45] It is also known that P53 and SMN interact and it has therefore been suggested that by binding P53, SMN stops P53 from activating apoptosis.[46] Thus, a lack of SMN could be

causing an increase in P53 and its downstream transcripts. Why then are the effects of this not seen until at least 6 months old, in the case of Type 1 SMA? Perhaps this is due to apoptosis being important in the development of the CNS and it is not until the requirement of apoptotic mechanisms in the CNS is decreased that the abnormal apoptosis activation is obvious.[47] In addition, it has been shown that caspases, which are important in apoptosis, can cleave SMN.[45] Perhaps if SMN is cleaved it is no longer be able to bind P53, and P53 can subsequently activate cell death. However, this is speculation and in fact it is unclear whether cleaving SMN abolishes its anti-apoptotic properties or whether it is the products created by cleaving SMN that can induce apoptosis.[47]

It is known that DNA damage can enhance P53 activity.[48] DNA repair mechanisms can detect and combat this damage and therefore, it would be possible that an increase in DNA repair could provide a level of resistance to cell death. Murray *et. al.* (Acta Neuropathol. Commun., *In Press*) showed that in resistant motor neurons there is an increase at the transcript level in DNA repair compared to vulnerable motor neurons. However, at the protein level, which was investigated here, there was no significant difference in DNA repair between resistant and vulnerable motor neurons. It is possible that although there is an increased level of transcript involved in DNA repair these are not translated into proteins as the regulation of gene expression continues even after transcription to ensure that protein homeostasis is maintained.[49]

However, it must be considered that perhaps it is the method used to investigate DNA repair at the protein level in this investigation is not optimal. Here, the entire spinal cord and brainstem were stained and motor neurons within the facial nuclei and thoracic region were imaged. It may be that some motor neurons imaged do not innervate the specific muscles which were defined are being highly vulnerable or resistant. Murray *et. al.* (Acta Neuropathol. Commun., *In Press*) injected a tracer into differentially vulnerable muscles to mark the motor neurons that correspond to the specific muscles. When these were stained for pH2AX and the intensity measured, this showed a decrease in pH2AX in vulnerable motor neurons of the thoracic spinal cord. Therefore, future methods that will take this variability into consideration

should be developed to investigate other markers of DNA repair before discounting the theory that DNA repair may provide resistance in neurodegeneration.

It should also be noted that wild type mice were used to analyse the brainstems and spinal cords for DNA repair markers rather than using an SMA mouse model. This allowed differences in these markers that normally occur between differentially vulnerable motor neurons to be studied to determine whether these differences may cause one cell to deal with additional stress, like a decrease in SMN protein, while another is unable to cope. Although there was no significant difference in these markers in the wild type mice at the protein level, it would still be interesting to further investigate DNA repair markers within SMA mouse models. It could be that the increased transcripts in resistant motor neurons are available and under the stress placed on these motor neurons in SMA the transcripts are translated into proteins.

Chapter 4: Re-deriving the *Smn*$^{2B/-}$ mouse model for investigation into cell death pathway activation

Introduction

There are various mouse models used in SMA research.[50,23,51] One of these models is the *Smn*$^{2B/-}$ mouse model of SMA that was created by mutating the murine *Smn* gene to generate the *Smn2B* allele.[21] This allele acts like *SMN2*, as the mutation is within exon 7, and when expressed on a null background it creates a mouse with a phenotype representative of SMA.[20] In the original manuscript, the *Smn*$^{2B/-}$ mouse was described as being an intermediate mouse model of SMA with a life expectancy of around 28 days.[20] It has a longer pre-symptomatic window in comparison to more severe mouse models, in which it displays a normal weight gain, making it indistinguishable from its littermates.[20] It is not until approximately P14 that *Smn*$^{2B/-}$ mice display phenotypic features of SMA.[20] At this point, they can be distinguished from littermates as their ears and tails look comparatively smaller and they weigh less.[20] At P21, denervation and pre-synaptic swelling is evident in the NMJs of *Smn*$^{2B/-}$ mice.[20] Furthermore, as in other models of SMA and in SMA patients, there is also differential vulnerability of muscles in *Smn*$^{2B/-}$ mice, with some muscle showing large amounts of these NMJ abnormalities and others showing very little or even no NMJ abnormalities.[20]

The *Smn*$^{2B/-}$ mouse model of SMA was used for the work presented in Chapter 1 as it had been used by Murray *et. al.* (Acta Neuropathol. Commun., *In Press*) in the work previously described. This model was used as they were able to make use of its prolonged pre-symptomatic period, in which NMJs remain intact, to utilise retrograde transport, whereby molecules are transported from the NMJ, along the axon and into the cell body. A tracer was injected into specific muscles and taken up by motor neurons at the NMJ. It was transported along the axon to highlight the cell bodies of motor neurons that correspond to these muscles.

In Chapter 1, it was shown by qRT-PCR that transcripts involved in cell death were up-regulated in both the *Smn*$^{2B/-}$ and the *Smn*$^{-/-}$;*SMN2*$^{(tg/0)}$ mouse models of SMA pre-

symptomatically. As previously mentioned, this is of interest due to this up-regulation occurring before any NMJ pathology is observed. This may suggest that the activation of cell death pathways, in the cell body, are causing NMJ pathology rather than the NMJ pathology causing the death of the cell.

In this chapter, I aimed to investigate the timing of cell death pathway activation in the $Smn^{2B/-}$ mouse model of SMA. To do this the $Smn^{2B/-}$ mouse model had to be re-derived, as this model was not available within our laboratory. The re-derived litter was created by crossing $Smn^{+/-}$ mice, which were on a FVB background, with $Smn^{2B/+}$ mice, which were on a C57BL6J background. Before use in experimental work, our $Smn^{2B/-}$ mice were characterised. Characterisation involved assessing phenotypic features and weight trends of the mice as well as analysing NMJ morphology at end stage of the disease and at P7. At this time point there was no evidence of morphological defects. However, the levels of key transcripts in the P53 signalling pathway revealed a significant up-regulation at P7. Finally, we attempted to optimise a dosing regime for the P53 inhibitor Pifithrin-α (PFT). This will allow for future efforts dedicated to investigating whether inhibition of the P53 signalling pathway can impact upon NMJ pathology.

Results

The steps involved in the re-derivation of the *Smn*$^{2B/-}$ mouse model of SMA can be seen in Figure 14. Firstly, *Smn*$^{2B/+}$ mice on a C57BL6J background were imported from the Kothary Laboratory and were crossed with C57BL6J wild type mice to produce *Smn*$^{2B/+}$ and *Smn*$^{+/+}$ mice. This allowed the colony to be expanded using the *Smn*$^{2B/+}$ mice. It also created the opportunity to optimise the genotyping protocol in our laboratory. PCR and gel electrophoresis amplified and separated DNA fragments that represented the *Smn2B* allele or murine *Smn*. While *Smn*$^{2B/+}$ mice displayed two bands, the *Smn2B* allele of 700bp and the murine *Smn* of 500bp, *Smn*$^{+/+}$ mice have only murine *Smn* and therefore were represented by one 500bp band (Figure 15A). *Smn*$^{2B/+}$ mice were subsequently crossed together to produce a litter containing *Smn*$^{2B/+}$, *Smn*$^{2B/2B}$ and *Smn*$^{+/+}$ mice. Genotyping revealed *Smn*$^{2B/+}$ mice and these were bred with *Smn*$^{+/-}$ mice on the FVB background, giving a litter that contained mixed background *Smn*$^{+/+}$, *Smn*$^{+/-}$, *Smn*$^{2B/+}$ and *Smn*$^{2B/-}$ mice. Genotyping this litter involved two steps. Firstly, the 2B genotyping protocol differentiated *Smn*$^{2B/+}$ and *Smn*$^{2B/-}$ mice (Figure 15A). However, *Smn*$^{+/-}$ and *Smn*$^{+/+}$ cannot be distinguished from this protocol as both display one 500bp band. Therefore, a protocol that amplifies the cassette that creates the null allele as well as amplifying murine *Smn* was subsequently performed (Figure 15B). *Smn*$^{+/-}$ mice display two bands, the murine *Smn* of 1050bp and the cassette of 950bp, whereas *Smn*$^{+/+}$ mice display only one band at 1050bp.

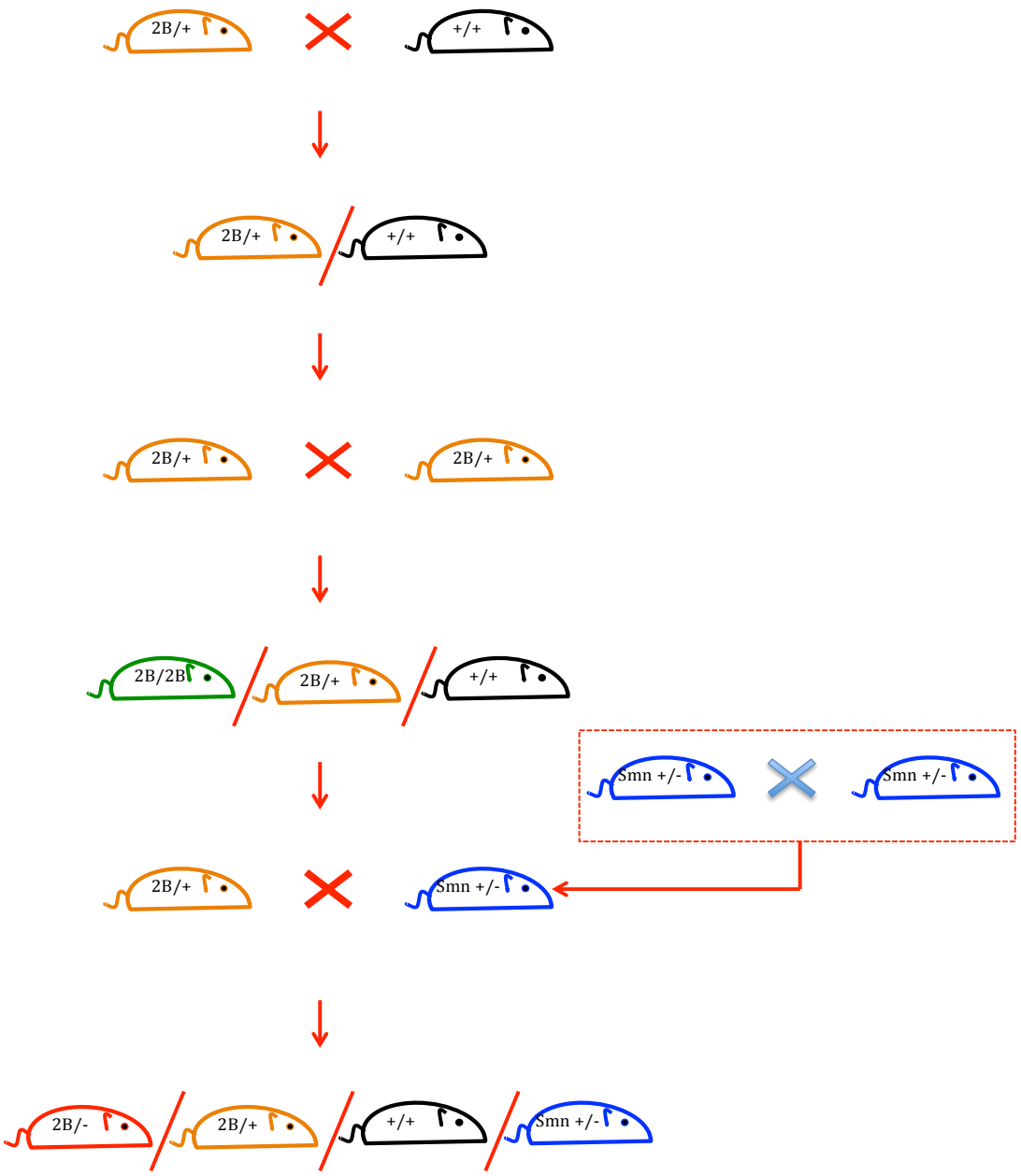

Figure 14: Re- derivation of the Smn$^{2B/-}$ mouse line. *C57BL6J Smn*$^{2B/+}$ mice were imported from the Kothary Laboratory. These were crossed with C57BL6J mice, homozygous for murine *Smn*. This produced litters consisting of *Smn*$^{2B/+}$ and *Smn*$^{+/+}$ mice. *Smn*$^{2B/+}$ mice were crossed together giving *Smn*$^{2B/2B}$, *Smn*$^{2B/+}$ and *Smn*$^{+/+}$ mice. In this project, *Smn*$^{2B/+}$, which were on a C57BL6J background, were crossed with *Smn*$^{+/-}$ mice, on a FVB background, to obtain a litter of *Smn*$^{2B/-}$, *Smn*$^{2B/+}$, *Smn*$^{+/-}$ and *Smn*$^{+/+}$ mice. *Smn*$^{2B/-}$ is the desired SMA model while *Smn*$^{+/+}$ mice can be used as wild type controls.

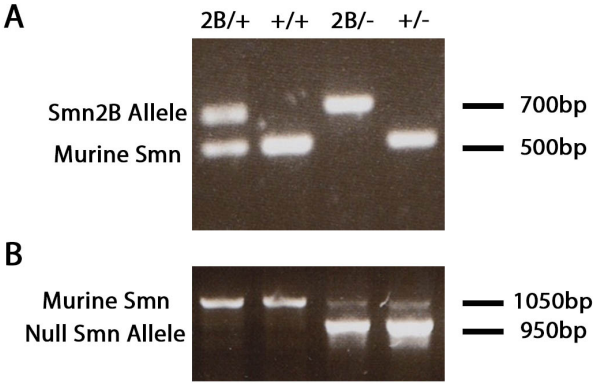

Figure 15: PCR and gel electrophoresis reveals the genotypes of mice in the re-derived *Smn*$^{2B/-}$ line. (A) The first PCR differentiates between *Smn*$^{2B/-}$ and *Smn*$^{2B/+}$ (top band = 700bp *Smn2B* allele; bottom band = 500bp murine *Smn*). (B) The second PCR differentiates between *Smn*$^{+/-}$ and *Smn*$^{+/+}$ mice (top band = 1050bp murine *Smn*; bottom band = 950bp null *Smn* allele [primers bind the cassette that is inserted into the *Smn* gene to render the gene non-functional]).

Characterisation of our *Smn*$^{2B/-}$ mice was subsequently carried out. The weights of our *Smn*$^{2B/-}$ mice and their littermates were tracked and subsequently plotted (Figure 16A). The graphs show the *Smn*$^{2B/-}$ mice are indistinguishable from each other early in post-natal life. However, when phenotypic features become apparent, weight gain in the *Smn*$^{2B/-}$ mice stalls and their weight decreases. Distinguishing features include small ears and a short tail, which are not obvious until approximately P12 (Figure 16B).

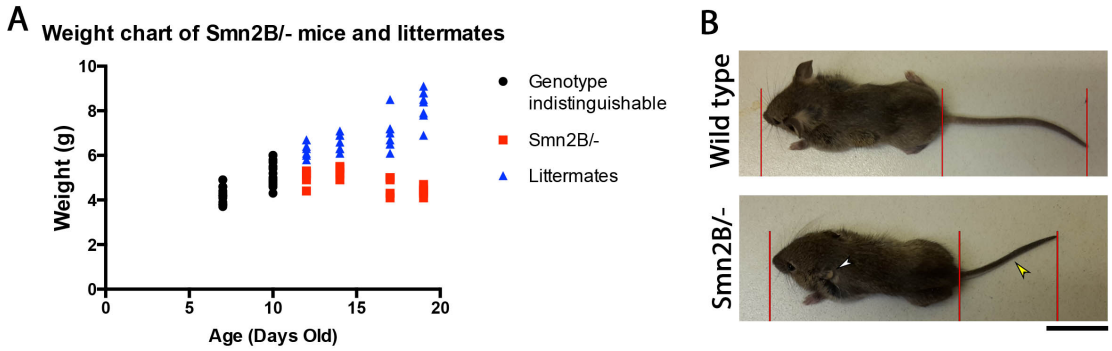

Figure 16: Phenotype of re-derived *Smn*$^{2B/-}$ mouse model of SMA. *Smn*$^{2B/-}$ mice show similar weight trends and phenotypic features as the previous *Smn*$^{2B/-}$ model. (A) The graph shows the weights of mice in a re-derived *Smn*$^{2B/-}$ litter. Note the divergence of weights from P12. When weighed, it was noted which mice displayed SMA features (small ears and a small tail), these are denoted by red squares. (B) Images show the differences between a *Smn*$^{2B/-}$ mouse and a wild type littermate. Note the abnormal ears (white arrowhead), the shorter, darker tail (yellow arrowhead) and the size difference (Approximate sizes: WT body = 60mm, WT tail = 48mm; *Smn*$^{2B/-}$ body = 55mm, *Smn*$^{2B/-}$ tail = 30mm) Scale Bar = 2cm.

We next analysed the morphology of NMJs from our *Smn*$^{2B/-}$ mice. Whole mount abdominal muscles were stained with α-Bungarotoxin to label endplates and staining for Neurofilament and Synaptic Vesicle 2 protein labelled axons. Abdominal muscles were used due to their accessibility and their thickness, which is small enough to permit staining and imaging of the entire muscle. Furthermore, in various mouse models of SMA the abdominal muscles are vulnerable and display severe NMJ pathology.[9,20] At P20, the *Smn*$^{2B/-}$ mice show denervation and pre-synaptic swelling in the Transversus Abdominis and Rectus Abdominis muscles, which is not apparent in wild type muscles (Figure 17). However, the NMJs of the Rectus Abdominis seemed to have more severe pre-synaptic swelling than the NMJs of the Transversus Abdominis. In general, NMJs of *Smn*$^{2B/-}$ mice display an immature appearance. Unlike the wild type NMJs that are mature and pretzel-like, the NMJs of *Smn*$^{2B/-}$ mice retain an immature, plaque-like appearance.[52] However, at P7 *Smn*$^{2B/-}$ mice are pre-symptomatic and show no obvious signs of abnormal NMJ morphology in the Transversus Abdominis. There was no apparent denervation or pre-synaptic

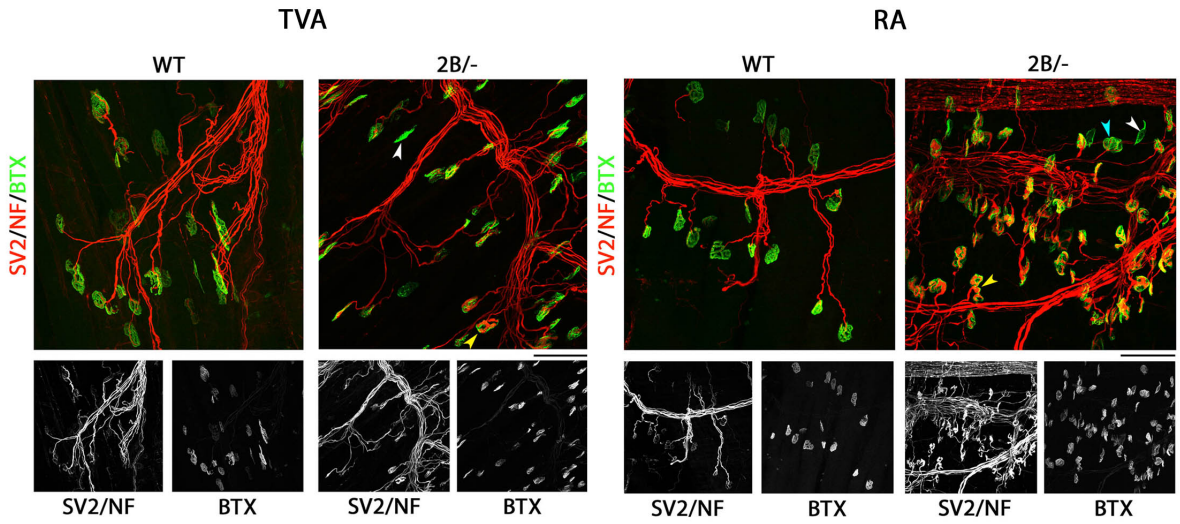

Figure 17: The NMJs of our *Smn*$^{2B/-}$ mice show signs of denervation and pre-synaptic swelling at P20. Representative confocal micrographs show the transversus abdominis (TVA) and rectus abdominis (RA) muscles from wild type (WT) and *Smn*$^{2B/-}$ mice (2B/-), both P20. Endplates are labelled with α-Bungarotoxin (BTX; green) and antibodies against Synaptic Vesicle Protein 2 (SV2) and Neurofilament (NF) allow visualization of axons (red). Note the fully innervated, pretzel-like appearance of the mature endplates in the wild type compared to the plaque-like appearance of the endplates in the *Smn*$^{2B/-}$. Denervation (white arrowhead), partial denervation (blue arrowhead) and pre-synaptic swelling (yellow arrowhead) can be seen. Scale bar = 50μm.

swelling. At this age, *Smn*$^{2B/-}$ and wild type mice have immature NMJs. The NMJs in both mice have a plaque-like appearance and some remain poly-innervated.

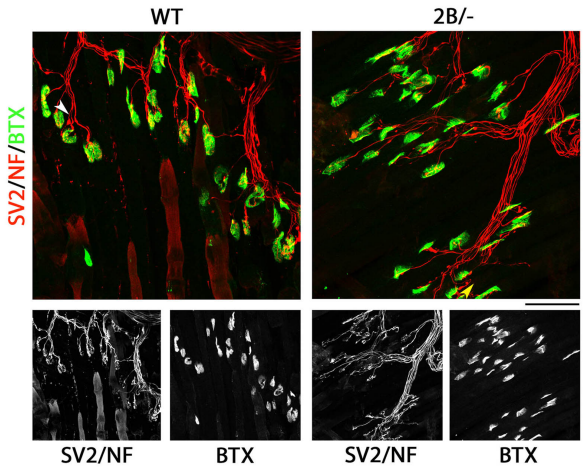

Figure 18: Transversus Abdominis NMJs of P7 *Smn*$^{2B/-}$ mice do not show signs of denervation or pre-synaptic swelling. Representative confocal micrographs show the transversus abdominis (TVA) from wild type (WT) and *Smn*$^{2B/-}$ mice (2B/-), both P7. Endplates are labelled with α-Bungarotoxin (green) and antibodies against Synaptic Vesicle Protein 2 (SV2) and Neurofilament (NF) allow visualization of axons (red). At this age, endplates still have an immature, plaque-like appearance in both wild type and *Smn*$^{2B/-}$ mice. Scale bar = 50μm.

Since there was no obvious NMJ defects or phenotypic features of SMA at P7, this was used as a pre-symptomatic time point. Transcriptional analysis by qRT-PCR was performed at P7 to investigate whether there is an early up-regulation of transcripts involved in the P53 signalling pathway in our *Smn*$^{2B/-}$ mice. Whole spinal cord cDNA of *Smn*$^{2B/-}$ mice and wild type littermates was used to compare *FAS*, *PMAIP1* and *CDKN1A* transcripts. All three transcripts were significantly up-regulated in the *Smn*$^{2B/-}$ mouse model of SMA compared to their wild type littermates (Figure 19). This confirms previous results performed on a genetically distinct version of the *Smn*$^{2B/-}$ mouse model, demonstrating an up-regulation of factors involved in the P53 signalling pathway at pre-symptomatic time points (see Figure 5&7). Importantly, this analysis was performed at P7, indicating that cell death pathway activation can be detected prior to evidence of NMJ pathology. Furthermore, this finding validates this model as an appropriate model to attempt to inhibit the activation of cell death pathways using PFT.

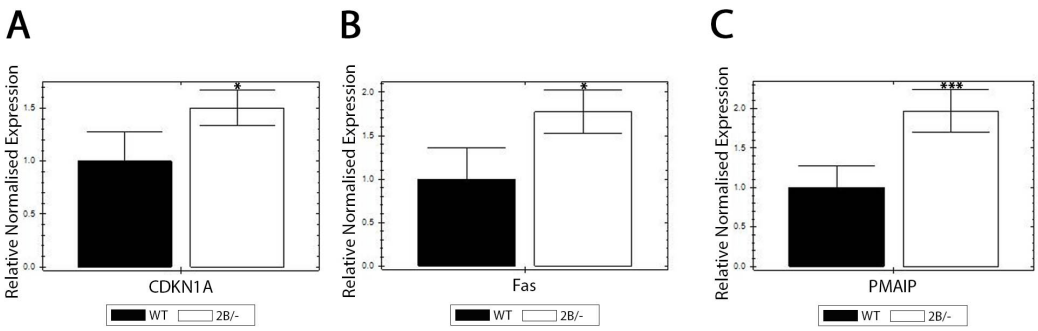

Figure 19: There is an up-regulation of transcripts involved in cell death in Smn$^{2B/-}$ mice at a pre-symptomatic stage. qRT-PCR analysis was used to compare the transcript levels of *CDKN1A*, *FAS* and *PMAIP1* in cDNA from *Smn*$^{2B/-}$ and control (WT) mice at P7 (pre-symptomatic). Bar charts (Mean ± SEM) show that the relative normalized expression of *CDKN1A* (A), *FAS* (B) and *PMAIP1* (C) are all significantly up-regulated in *Smn*$^{2B/-}$ mice compared to wild type controls at P7 (*P<0.05, ***P<0.001 by Mann Whitney U Test; n=4 mice per genotype).

Several litters were treated between P5 and P9 with PFT and while one half of the litter received PFT, the other half acted as a control group. However, following retrieval of the spinal cords, genotyping revealed that there were no *Smn*$^{2B/-}$ mice in any of the treated litters. This was performed in 3 litters of mice and, although statistically unlikely, there were no *Smn*$^{2B/-}$ mice in any of the treated litters. For this reason, this work is on going and current efforts are dedicated at repeating this work in *Smn*$^{2B/-}$ mice. Once samples of cDNA from the spinal cord of treated and untreated *Smn*$^{2B/-}$ mice are acquired, qRT-PCR will compare the levels of transcripts involved in cell death between the two. This will assess whether PFT treatment can alter the regulation of cell death transcripts.

Discussion

The *Smn*$^{2B/-}$ mouse model of SMA has been re-derived, creating a *Smn*$^{2B/-}$ mouse on a mixed genetic background. This mouse model appears to have very similar features to the original *Smn*$^{2B/-}$ mouse that was on a pure genetic background. These similarities are in phenotypic features, weight trends, NMJ pathology and regulation of cell death transcripts. Both models have small ears and tails and show a normal weight gain before reaching a point at which weight gain stops and weight begins to decrease.[20] They both show denervation and pre-synaptic swelling at the NMJs within abdominal muscles and both have an up-regulation of transcripts involved in cell death, pre-symptomatically.[20,15]

PFT was to be used to assess whether the levels of transcripts involved in cell death could be altered in *Smn*$^{2B/-}$ mice. PFT is a drug originally developed to provide a treatment to reduce the side effects of chemotherapy, which are mainly caused by apoptosis through the P53 signalling pathway.[53] It has also been shown to decrease the activation of *CDKN1A* which occurs downstream of P53.[53] Due to a lack of *Smn*$^{2B/-}$ mice within litters, it is still unknown whether PFT is able to decrease transcripts involved in cell death in the spinal cords of *Smn*$^{2B/-}$ mice. Therefore, the progression of this project will depend on the outcome of the experiments. If in the PFT trial that we aimed to carry out, PFT does not alter the levels of these transcripts in the spinal cords of *Smn*$^{2B/-}$ mice, it should be considered that either the dose of PFT administered is not effective or PFT does not successfully cross the blood brain barrier (BBB). The PFT dose used in this experiment was previously used in mice to reduce cancer treatment side effects and also to reduce cell death in neurons of the cerebral cortex.[53,54] It is also known that when given to mice via intraperitoneal injection, PFT is detectable in the cerebrospinal fluid of mice after 30 minutes and therefore PFT is able to successfully cross the BBB.[54] However, in order to investigate whether PFT is crossing the BBB in our mouse model, transcript levels in another tissue, muscle for example, in which PFT would be able to cross into, should be compared in treated and untreated mice. An alteration in transcripts in the muscle of treated mice would indicate that manipulating drug entry through the BBB,

perhaps pharmacologically, might be required for PFT to act on spinal cord tissue. Gyroxin, which alters the permeability of the BBB for a short period of time, could be considered for use.[55] However, if the PFT trial showed that PFT can alter transcript levels in the spinal cord, *Smn*$^{2B/-}$ mice would be treated for a longer period of time and the impact of decreasing transcripts involved in cell death on NMJ pathology would be assessed.

The lack of *Smn*$^{2B/-}$ mice is the main limitation of this study. Therefore, in the future, perhaps *Smn*$^{2B/-}$ mice should be created by crossing *Smn*$^{+/-}$ with *Smn*$^{2B/2B}$ mice. This would give a 50% chance of obtaining *Smn*$^{2B/-}$ mice, rather than the 25% chance that we had in this project. Although, there was only a 25% chance, the cross that was carried out for this project produced *Smn*$^{+/+}$ mice and *Smn*$^{2B/-}$ mice in the same litter. These *Smn*$^{+/+}$ littermates could then be used as wild type controls. Furthermore, the *Smn*$^{2B/-}$ mice were re-derived onto the FVB background and on this background mice are often more efficient breeders and have larger litter sizes.[56] It was therefore expected that there would be a greater chance of having *Smn*$^{2B/-}$ mice within one litter.

Overall, establishing the *Smn*$^{2B/-}$ mouse model within our laboratory was successful and it is a valuable model for future experimentation. The presence of abnormal NMJ morphology was confirmed and this correlates with disease onset and progression. The early up-regulation of cell death transcripts was also confirmed in our *Smn*$^{2B/-}$ mice pre-symptomatically, at P7. This is important as it suggests that the activation of cell death pathways may contribute to the degeneration of the motor neuron and therefore, warrants further investigation into this idea.

Chapter 5: Conclusions and Future Work

There were two main parts to this project. Firstly, work was carried out to discover whether transcriptional differences between differentially vulnerable motor neuron populations that had been highlighted by Murray *et. al*. (Acta Neuropathol. Commun., *In Press*) through RNAseq were detectable by other methods. These methods included qRT-PCR and immunofluorescence. Transcriptional differences that occurred between pre-symptomatic (P10) $Smn^{2B/-}$ and wild type motor neurons were investigated by qRT-PCR. These transcripts included those involved in rRNA binding, ubiquitination and cell death. qRT-PCR detected a down-regulation of *UBB*, involved in ubiquitination, and up-regulation of *FAS*, *CDKN1A* and *PMAIP1*, which are transcripts associated with cell death. There was no detectable difference in *MRPL20* and *RPS27A* transcript levels, both associated with rRNA binding, between wild type and $Smn^{2B/-}$ mice by qRT-PCR. Transcriptional differences in DNA repair that had occurred between vulnerable and resistant pools of motor neurons, in both wild type and $Smn^{2B/-}$ mice, were investigated by immunofluorescence. Staining for markers of DNA repair and measuring the staining intensity could represent the level of DNA repair activity. There was found to be no significant difference in staining intensity between resistant, brainstem motor neurons and vulnerable, spinal cord motor neurons.

Detecting these transcriptional differences by qRT-PCR or by immunofluorescence would strengthen the suggestion that alterations in these functional clusters do occur in the $Smn^{2B/-}$ mouse model. In turn, this could warrant further investigation into why or how these functional clusters may be impacting on SMA pathology. Detecting changes in not only one but two mouse models of SMA, the intermediate $Smn^{2B/-}$ mouse model and the severe $Smn^{-/-};SMN2^{(tg/0)}$ mouse model, suggests that these transcriptional changes are not exclusive to the $Smn^{2B/-}$ model but rather they may be universal to SMA mouse models and in fact could occur in patients.

In particular, transcripts involved in cell death were up-regulated in both mouse models of SMA. This was pre-symptomatically and therefore before any NMJ pathology is apparent. This suggests that the activation of cell death pathways may

contribute to the degeneration of the motor neuron, with the NMJ simply being the most vulnerable part of the cell and therefore the part where the effects of cell death activation are first observed. Preliminary work was carried out to begin investigation into this theory. We attempted to assess whether PFT can alter cell death transcripts in our *Smn*$^{2B/-}$ mouse model. The result from this would have established whether there is a possibility of PFT treatment impacting on NMJ pathology, perhaps reducing denervation or pre-synaptic swelling. The idea behind this experiment is that this may extend the pre-symptomatic period, which would in turn give a longer period of time in which therapeutics, perhaps those that restore SMN, could be administered.

In the future, we first need to establish whether the current PFT dose can reduce the levels of cell death transcripts that are currently up-regulated in vulnerable *Smn*$^{2B/-}$ motor neurons by qRT-PCR. If PFT does alter cell death transcripts, then PFT should be administered for various lengths of time to assess the effects on NMJ pathology, specifically denervation and pre-synaptic swelling. Subsequently, if PFT is able to reduce NMJ pathology in *Smn*$^{2B/-}$ mice, we should consider investigating the possibility that down regulating cell death transcripts could extent the time window in which restorative SMN therapies can be given. *Smn*$^{Res/Res}$ mice (*SMN2;Smn*$^{\Delta 7}$*;Cre-ER;Smn*$^{Res/Res}$) are an inducible SMA mouse model in which SMN production can be restored.[57] Restoring SMN is most effective early on in the disease.[57] However, if these mice were treated with PFT, is it possible that the time window that is effective for restoring SMN in order to alter the SMA phenotype would be extended? This idea should be investigated. By carrying out this work we would not only strengthen the theory that the early up-regulation of cell death pathways are the causative factor of NMJ pathology in SMA but also give valuable knowledge that could be used in the therapeutic treatment of SMA patients.

References

1. Pearn, J. Incidence, prevalence, and gene freqequency studies of chronic childhood spinal muscular atrophy. (1978). at <http://jmg.bmj.com/content/15/6/409.full.pdf+html>

2. Munsat, T. L. International SMA Collaboration. *Neuromuscul. Disord.* **1,** 81 (1991).

3. Lefebvre, S. Identification and characterization of a spinal muscular atrophy-determining gene. *Cell* **80,** 155–165 (1995).

4. Sleigh, J. N., Gillingwater, T. H. & Talbot, K. The contribution of mouse models to understanding the pathogenesis of spinal muscular atrophy. *Dis. Model. Mech.* **4,** 457–67 (2011).

5. Lorson, C. L., Hahnen, E., Androphy, E. J. & Wirth, B. A single nucleotide in the SMN gene regulates splicing and is responsible for spinal muscular atrophy. *Proc. Natl. Acad. Sci.* **96,** 6307–6311 (1999).

6. Butchbach, M. E. R. & Burghes, A. H. M. Perspectives on models of spinal muscular atrophy for drug discovery. *Drug Discov. Today Dis. Model.* **1,** 151–156 (2004).

7. Hamilton, G. & Gillingwater, T. H. Spinal muscular atrophy: going beyond the motor neuron. *Trends Mol. Med.* **19,** 40–50 (2013).

8. Mailman, M. D. *et al.* Molecular analysis of spinal muscular atrophy and modification of the phenotype by SMN2. *Genet. Med.* **4,** 20–6 (2002).

9. Murray, L. M. *et al.* Selective vulnerability of motor neurons and dissociation of pre- and post-synaptic pathology at the neuromuscular junction in mouse models of spinal muscular atrophy. *Hum. Mol. Genet.* **17,** 949–62 (2008).

10. Gavrilina, T. O. *et al.* Neuronal SMN expression corrects spinal muscular atrophy in severe SMA mice while muscle-specific SMN expression has no phenotypic effect. *Hum. Mol. Genet.* **17,** 1063–75 (2008).

11. Rudnik-Schoneborn, S. *et al.* Congenital heart disease is a feature of severe infantile spinal muscular atrophy. *J. Med. Genet.* **45,** 635–638 (2008).

12. Kong, L. *et al.* Impaired synaptic vesicle release and immaturity of neuromuscular junctions in spinal muscular atrophy mice. *J. Neurosci.* **29,** 842–51 (2009).

13. Kariya, S. *et al.* Reduced SMN protein impairs maturation of the neuromuscular junctions in mouse models of spinal muscular atrophy. *Hum. Mol. Genet.* **17,** 2552–69 (2008).

14. Jones, H. R., Vivo, D. C. De & Darras, B. T. *Neuromuscular Disorders of Infancy, Childhood, and Adolescence: A Clinician's Approach*. (Butterworth-Heinemann, 2003). at <https://books.google.com/books?hl=en&lr=&id=ilPXTTWImh4C&pgis=1>

15. Murray, Lyndsay M; Beauvais, Ariane; Gibeault, Sabrina; Courtney, Natalie L; Kothary, R. Transcriptional Profiling of Differentially Vulnerable Motor Neurons at Pre-symptomatic Stage in the Smn2B/- Mouse Model of Spinal Muscular Atrophy. *Acta Neuropathol. Commun.*

16. Boyer, J. G. *et al.* Myogenic program dysregulation is contributory to disease pathogenesis in spinal muscular atrophy. *Hum. Mol. Genet.* **23,** 4249–59 (2014).

17. Zhang, Z. *et al.* SMN deficiency causes tissue-specific perturbations in the repertoire of snRNAs and widespread defects in splicing. *Cell* **133,** 585–600 (2008).

18. Zhao, S., Fung-Leung, W.-P., Bittner, A., Ngo, K. & Liu, X. Comparison of RNA-Seq and microarray in transcriptome profiling of activated T cells. *PLoS One* **9,** e78644 (2014).

19. Staropoli, J. F. *et al.* Rescue of gene-expression changes in an induced mouse model of spinal muscular atrophy by an antisense oligonucleotide that promotes inclusion of SMN2 exon 7. *Genomics* **105,** 220–8 (2015).

20. Bowerman, M., Murray, L. M., Beauvais, A., Pinheiro, B. & Kothary, R. A critical smn threshold in mice dictates onset of an intermediate spinal muscular atrophy phenotype associated with a distinct neuromuscular junction pathology. *Neuromuscul. Disord.* **22,** 263–76 (2012).

21. Hammond, S. M. *et al.* Mouse survival motor neuron alleles that mimic SMN2 splicing and are inducible rescue embryonic lethality early in development but not late. *PLoS One* **5,** e15887 (2010).

22. Schrank, B. *et al.* Inactivation of the survival motor neuron gene, a candidate gene for human spinal muscular atrophy, leads to massive cell death in early mouse embryos. *Proc. Natl. Acad. Sci.* **94,** 9920–9925 (1997).

23. Hsieh-Li, H., Chang, J., Jong, Y. & Wu, M. A mouse model for spinal muscular atrophy. *Nat. ...* **24,** 66–70 (2000).

24. Pellizzoni, L., Kataoka, N., Charroux, B. & Dreyfuss, G. A Novel Function for SMN, the Spinal Muscular Atrophy Disease Gene Product, in Pre-mRNA Splicing. *Cell* **95,** 615–624 (1998).

25. Burghes, A. H. M. & Beattie, C. E. Spinal muscular atrophy: why do low levels of survival motor neuron protein make motor neurons sick? *Nat. Rev. Neurosci.* **10,** 597–609 (2009).

26. Li, D. K., Tisdale, S., Lotti, F. & Pellizzoni, L. SMN control of RNP assembly: from post-transcriptional gene regulation to motor neuron disease. *Semin. Cell Dev. Biol.* **32,** 22–9 (2014).

27. Gabanella, F. *et al.* Ribonucleoprotein assembly defects correlate with spinal muscular atrophy severity and preferentially affect a subset of spliceosomal snRNPs. *PLoS One* **2,** e921 (2007).

28. Lotti, F. *et al.* An SMN-dependent U12 splicing event essential for motor circuit function. *Cell* **151,** 440–54 (2012).

29. Bäumer, D. *et al.* Alternative splicing events are a late feature of pathology in a mouse model of spinal muscular atrophy. *PLoS Genet.* **5,** e1000773 (2009).

30. Rossoll, W. Specific interaction of Smn, the spinal muscular atrophy determining gene product, with hnRNP-R and gry-rbp/hnRNP-Q: a role for Smn in RNA processing in motor axons? *Hum. Mol. Genet.* **11,** 93–105 (2002).

31. Bowerman, M. *et al.* SMN, profilin IIa and plastin 3: a link between the deregulation of actin dynamics and SMA pathogenesis. *Mol. Cell. Neurosci.* **42,** 66–74 (2009).

32. Dubowitz, V. Very severe spinal muscular atrophy (SMA type 0): an expanding clinical phenotype. *Eur. J. Paediatr. Neurol.* **3,** 49–51 (1999).

33. Brockington, A. *et al.* Unravelling the enigma of selective vulnerability in neurodegeneration: motor neurons resistant to degeneration in ALS show distinct gene expression characteristics and decreased susceptibility to excitotoxicity. *Acta Neuropathol.* **125,** 95–109 (2013).

34. Murray, L. M. *et al.* Pre-symptomatic development of lower motor neuron connectivity in a mouse model of severe spinal muscular atrophy. *Hum. Mol. Genet.* **19,** 420–33 (2010).

35. Murray, L. M., Beauvais, A., Bhanot, K. & Kothary, R. Defects in neuromuscular junction remodelling in the Smn(2B/-) mouse model of spinal muscular atrophy. *Neurobiol. Dis.* **49,** 57–67 (2013).

36. Wishart, T. M. *et al.* Dysregulation of ubiquitin homeostasis and β-catenin signaling promote spinal muscular atrophy. *J. Clin. Invest.* **124,** 1821–34 (2014).

37. Chowdhury, D. *et al.* gamma-H2AX dephosphorylation by protein phosphatase 2A facilitates DNA double-strand break repair. *Mol. Cell* **20,** 801–9 (2005).

38. Sharma, A., Singh, K. & Almasan, A. Histone H2AX phosphorylation: a marker for DNA damage. *Methods Mol. Biol.* **920,** 613–26 (2012).

39. Schultz, L. B., Chehab, N. H., Malikzay, A. & Halazonetis, T. D. p53 binding protein 1 (53BP1) is an early participant in the cellular response to DNA double-strand breaks. *J. Cell Biol.* **151,** 1381–90 (2000).

40. Ward, I. M., Minn, K., van Deursen, J. & Chen, J. p53 Binding Protein 53BP1 Is Required for DNA Damage Responses and Tumor Suppression in Mice. *Mol. Cell. Biol.* **23,** 2556–2563 (2003).

41. De Planell-Saguer, M., Schroeder, D. G., Rodicio, M. C., Cox, G. A. & Mourelatos, Z. Biochemical and genetic evidence for a role of IGHMBP2 in the translational machinery. *Hum. Mol. Genet.* **18,** 2115–26 (2009).

42. Guenther, U.-P. *et al.* IGHMBP2 is a ribosome-associated helicase inactive in the neuromuscular disorder distal SMA type 1 (DSMA1). *Hum. Mol. Genet.* **18,** 1288–300 (2009).

43. Korhonen, L. The ubiquitin proteasome system in synaptic and axonal degeneration: a new twist to an old cycle. *J. Cell Biol.* **165,** 27–30 (2004).

44. Conforti, L., Adalbert, R. & Coleman, M. P. Neuronal death: where does the end begin? *Trends Neurosci.* **30,** 159–66 (2007).

45. Kerr, D. A., Nery, J. P., Traystman, R. J., Chau, B. N. & Hardwick, J. M. Survival motor neuron protein modulates neuron-specific apoptosis. *Proc. Natl. Acad. Sci. U. S. A.* **97,** 13312–7 (2000).

46. Young, P. J. *et al.* A direct interaction between the survival motor neuron protein and p53 and its relationship to spinal muscular atrophy. *J. Biol. Chem.* **277,** 2852–9 (2002).

47. Anderton, R. S., Meloni, B. P., Mastaglia, F. L. & Boulos, S. Spinal muscular atrophy and the antiapoptotic role of survival of motor neuron (SMN) protein. *Mol. Neurobiol.* **47,** 821–32 (2013).

48. Sakaguchi, K. *et al.* DNA damage activates p53 through a phosphorylation-acetylation cascade. *Genes Dev.* **12,** 2831–2841 (1998).

49. Shyu, A.-B., Wilkinson, M. F. & van Hoof, A. Messenger RNA regulation: to translate or to degrade. *EMBO J.* **27,** 471–81 (2008).

50. Monani, U. R. *et al.* The human centromeric survival motor neuron gene (SMN2) rescues embryonic lethality in Smn –/– mice and results in a mouse with spinal muscular atrophy. **9,** 333–340 (2000).

51. Le, T. T. *et al.* SMNDelta7, the major product of the centromeric survival motor neuron (SMN2) gene, extends survival in mice with spinal muscular atrophy and associates with full-length SMN. *Hum. Mol. Genet.* **14,** 845–57 (2005).

52. Sanes, J. R. & Lichtman, J. W. Induction, assembly, maturation and maintenance of a postsynaptic apparatus. *Nat. Rev. Neurosci.* **2,** 791–805 (2001).

53. Komarov, P. G. A Chemical Inhibitor of p53 That Protects Mice from the Side Effects of Cancer Therapy. *Science (80-.).* **285,** 1733–1737 (1999).

54. Culmsee, C. *et al.* A synthetic inhibitor of p53 protects neurons against death induced by ischemic and excitotoxic insults, and amyloid β-peptide. *J. Neurochem.* **77,** 220–228 (2008).

55. Alves da Silva, J. A., Oliveira, K. C. & Camillo, M. A. P. Gyroxin increases blood-brain barrier permeability to Evans blue dye in mice. *Toxicon* **57,** 162–7 (2011).

56. Szade, A. *et al.* Effect of crossing C57BL/6 and FVB mouse strains on basal cytokine expression. *Mediators Inflamm.* **2015,** 762419 (2015).

57. Lutz, C. M. *et al.* Postsymptomatic restoration of SMN rescues the disease phenotype in a mouse model of severe spinal muscular atrophy. *J. Clin. Invest.* **121,** 3029–41 (2011).

Publications and Presentations

Published Manuscripts:

Murray LM, Beauvais A, Gibeault S, **Courtney NL**, Kothary R (Acta Neuropathologica Communications, *In Press*) Transcriptional profiling of differentially vulnerable motor neurons at a pre-symptomatic stage in the *Smn*$^{2B/-}$ mouse model of spinal muscular atrophy.

Poster Presentations:

Courtney NL, Beauvais A, Gibeault S, Kothary R, Murray LM (2015, June) Pre-symptomatic analysis of motor neurons in mouse models of spinal muscular atrophy reveals an early up-regulation of cell death pathways. Poster presented at the Annual SMA Conference, Kansas City, MO, USA.

Courtney NL, Kothary R, Murray LM (2015, April) Investigating the factor regulating differential vulnerability of motor neurons in mouse models of spinal muscular atrophy. Poster presented at the British Neuroscience Association 2015 Festival of Neuroscience, Edinburgh, UK.

Courtney NL, Kothary R, Murray LM (2015, March) Investigating the factor regulating differential vulnerability of motor neurons in mouse models of spinal muscular atrophy. Poster presented at the Edinburgh Neuroscience Day 2015, Edinburgh, UK.

Oral Presentations:

Courtney NL, Murray LM (2014, December) Differential vulnerability of motor neurons in spinal muscular atrophy. Presented at a collaborative lab meeting.

Courtney NL, Murray LM (2015, May) Re-deriving the *Smn*$^{2B/-}$ mouse model of SMA. Presented at a collaborative lab meeting.